MODIFIED 3D SENSITIVITY MATRIX METHOD AND USE OF MULTICHANNEL CURRENT SOURCE FOR MAGNETIC RESONANCE ELECTRICAL IMPEDANCE TOMOGRAPHY (MREIT)

A THESIS

SUBMITTED TO THE DEPARTMENT OF ELECTRICAL AND ELECTRONICS ENGINEERING

AND THE GRADUATE SCHOOL OF ENGINEERING AND SCIENCES OF BILKENT UNIVERSITY

IN PARTIAL FULLFILMENT OF THE REQUIREMENTS FOR THE DEGREE OF

MASTER OF SCIENCE

By

Mustafa Rıdvan CANTAŞ

January 2012

I certify that I have read this thesis and that in my opinion it is fully adequate, in scope and in quality, as a thesis for the degree of Master of Science.

_____

Prof. Dr. Yusuf Ziya İder (Supervisor)

I certify that I have read this thesis and that in my opinion it is fully adequate, in scope and in quality, as a thesis for the degree of Master of Science.

_____

Prof. Dr. Ergin Atalar

I certify that I have read this thesis and that in my opinion it is fully adequate, in scope and in quality, as a thesis for the degree of Master of Science.

_____

Prof. Dr. Murat Eyuboğlu

Approved for the Graduate School of Engineering and Sciences:

_____

Prof. Dr. Levent Onural

Director of Graduate School of Engineering and Sciences

ABSTRACT

MODIFIED 3D SENSITIVITY MATRIX METHOD AND USE OF MULTICHANNEL CURRENT SOURCE FOR MAGNETIC RESONANCE ELECTRICAL IMPEDANCE TOMOGRAPHY (MREIT)

Mustafa Rıdvan CANTAŞ
M.S. in Electrical and Electronics Engineering
Supervisor: Prof. Dr.Yusuf Ziya İder

January 2012

Magnetic Resonance Electrical Impedance Tomography (MREIT) is a technique to image the electrical conductivity distribution inside the object (such as a human body). This technique consists of three steps: current injection into the object, the measurement of the magnetic flux density by a Magnetic Resonance Imaging (MRI) system, and the reconstruction of the conductivity distribution from the measured magnetic flux density. Although there are other algorithms to reconstruct the conductivity distribution inside the object, in this thesis, the Sensitivity Matrix Method is investigated for 3D problems. In MREIT, the use of the Sensitivity Matrix Method is not common for 3D problems. This is because of the fact that for 3D problems the Sensitivity Matrix Method requires large memory space and long calculation time. Calculation of the sensitivity matrix is the most time consuming part of this method. Therefore in this thesis, a modification is proposed in order to reduce the calculation time of the sensitivity matrix. Since the sensitivity matrix will be calculated at each iteration, this modification speeds up the algorithm significantly. Also by making several assumptions regarding the conductivity distribution of the object, the problem may be further reduced. In this thesis, conductivity distribution inside the object

is assumed to be z-invariant (z is the direction of the main magnetic field of the MRI system).Thus the dimension of the sensitivity matrix and the time required to calculate the conductivity distribution inside the object significantly decrease. Another problem with the application of the Sensitivity Matrix Method is that the magnetic flux density calculated by subtracting the calculated magnetic flux density (for the assumed initial conductivity distribution) from the measured one has errors. These erros are results of the boundary mismatches between the simulation object and the real object, inaccuracies in calculations and measurement artifacts. In this thesis, use of a multichannel current source is proposed in order to reduce these errors. Using the multichannel current source not only reduces the errors due to the boundary mismatches and other reasons but also sustains a nearly uniform current distribution inside the object.

Keywords: Magnetic Resonance Electrical Impedance Tomography (MREIT), Magnetic Resonance Imaging (MRI), Multichannel Current Source, Sensitivity Matrix Method (SMM) , Modified Sensitivity Matrix Method (MSMM)

ÖZET

DEĞİŞTİRİLMİŞ 3B HASSASİYET MATRİSİ METODU VE ÇOK KANALLI AKIM KAYNAĞININ MANYETİK REZONANS ELEKTRİKSEL EMPEDANS TOMOGRAFİ (MREET) İÇİN KULLANILMASI

Msutafa Rıdvan CANTAŞ
Elektrik ve Elektronik Mühendisliği Bölümü Yüksek Lisans
Tez Yöneticisi: Prof. Dr. Yusuf Ziya İder
Ocak 2012

Manyetik Rezonans Elektriksel Empedans Tomografi (MREET) bir cism (örneğin insan vücudu) içerisindeki elektriksel iletkenlik dağılımını görüntülemek için kullanılan bir yöntemdir. Bu yöntem üç aşamadan oluşmaktadır: cisime akım uygulanması, manyetik akı yoğunluğunun Manyetik Rezonans Görüntüleme sistemi ile ölçülmesi ve ölçülen manyetik akı yoğunluğundan iletkenlik dağılımının oluşturulması. Her ne kadar, cisimin elektriksel iletkenlik dağılımını oluşturmak için başka algoritmalar olsa da bu tezde Hassasiyet Matrisi Metodu üç boyutlu (3B) problemler için incelenecektir. Hassasiyet Matrisi Metodu, MREET'de 3B problemler için yaygın olarak kullanılan bir yöntem değildir çünkü Hassasiyet Matrisi Metodu'nun üç boyutlu problemlerde uygulanması için gereken bilgisayar hafızası ve zaman oldukça fazladır. Hassasiyet matrisinin hesaplanması, bu yöntemin en çok zaman alan kısmıdır. Dolayısıyla bu tezde hassasiyet matrisinin hesaplanma süresini düşüren bir değişiklik önerilmiştir. Hassasiyet matrisi her yenileme basamağında hesaplandığı için, bu değişiklik algoritmayı önemli ölçüde hızlandıracaktır. Ayrıca iletkenlik dağılımı için varsayımlar yapılarak çözümü kolaylaştırmak mümkündür. Bu tezde cisimin içerisindeki iletkenlik dağılımının z den (z MRG sisteminin ana manyetik alan yönüdür) bağımsız olduğu kabul edilmiştir.

Böylece hassasiyet matrisinin boyutu küçülmekte ve cisim içerindeki iletkenlik dağılımının hesaplanması için gereken süre önemli ölçüde azalmaktadır. Hassasiyet Matrisi Metodu'nun uygulanmasında karşılaşılan bir başka problem ise varsayılan ilk iletkenlik değeri için hesaplanan manyetik akı yoğunluğu, ölçülen manyetik akı yoğunluğundan çıkartıldığında, elde edilen manyetik akı yoğunlunda hataların olmasıdır. Bu hatalar simülasyonda kullanılan cisimle gerçekte kullanılan cismin kenar bilgilerinin örtüşmemesinden, simülasyonda yapılan hesaplardaki hatalardan ya da ölçümlerdeki yanlışlardan kaynaklanabilmektedir. Bu tezde, bu hataları azaltmak için çok kanallı akım kaynağının kullanılması önerilmiştir. Çok kanallı akım kaynağı bu hataları azaltmakla kalmayıp cisim içerisinde neredeyse homojen bir akım dağılımı sağlamaktadır.

Anahtar Kelimeler: Manyetik Rezonans Elektriksel Empedans Tomografi (MREET), Manyetik Rezonans Görüntüleme (MRG), Çok Kanallı Akım Kaynağı, Hassasiyet Matrisi Metodu (HMM), Değiştirilmiş Hassasiyet Matrisi Metodu (DHMM)

Acknowledgements

I would like to thank the people who made this thesis possible.

In the first place, it is my pleasure to express my thanks to Prof. Dr. Yusuf Ziya Ider for his invaluable guidance and support throughout my studies. I would also like to thank Prof. Dr. Ergin Atalar and Prof. Dr. Murat Eyüboğlu for accepting to be a member of my thesis jury. My parents Ceylan and Sultan Cantaş, and my siblings Gökhan and Meltem deserve special mention for their support and encouragement. I also want to thank my colleagues and friends Necip Gürler, Fatih Hafalır, Merve Begüm Terzi, and Haşim Meriç for giving me pleasant time when working with them. My special thanks are owed to Ömer Faruk Oran for his support and friendship. Finally, I wish to thank my girlfriend Nermin Kondakçı for her support and patience.

Table of Contents

List of Figures

List of Tables

Chapter 1 : Introduction

Magnetic Resonance Electrical Impedance Tomography (MREIT) is a technique to image electrical conductivity distribution inside the object. In medical imaging, human body is used as an object to be imaged. Since the electrical conductivity of the different cells and the tissues of the body have different electrical conductivity, this method can be used as an another contrast in the MRI system. Also some of the cancerous tissues can have different conductivity values than the healthy ones [1]-[3]. Therefore, the use of MREIT might be a helpful tool in the detection of the cancerous tissues in the body.

In MREIT it is necessary to inject current into the object. Current injection is made into the object by surface electrodes placed over the object. The injected current into the body, creates a magnetic flux around it. If the z is the direction of the main magnetic field of the MRI system, the z component of the magnetic flux density ($\mathbf{B}_z$) inside the object can be measured by the Magnetic Resonance Imaging (MRI) System. After acquiring the $\mathbf{B}_z$ distribution, the conductivity distribution of the object can be reconstructed from this $\mathbf{B}_z$ distribution. There are several algorithms to reconstruct conductivity distribution of the object from the measured $\mathbf{B}_z$**.** The Sensitivity Matrix Method which is discussed in this thesis, is one of them.

The relation between the magnetic flux density generated by the internal current distribution and the conductivity of an element is nonlinear. Therefore, in order to easily calculate the conductivity distribution from the magnetic flux density measurements, it is necessary to linearize the forward problem. Here the forward problem is defined as the calculation of the magnetic flux density which is produced by the internal current density of the object. If the forward problem is linearized around an initial conductivity distribution, the relation between the

magnetic flux density and the conductivity will be $\mathbf{B_z} = \mathbf{D}(\boldsymbol{\sigma})\boldsymbol{\sigma}$ (usually a uniform conductivity distribution is chosen as an initial conductivity distribution). If the forward problem is solved with the Finite Element Method (FEM), then the object is divided into N finite element. For M $\mathbf{B_z}$ measurement points the size of the $\mathbf{D}$ matrix will be MxN. Here the $\mathbf{D}$ matrix is called as the sensitivity matrix.

In 1998 the sensitivity matrix method is applied to MREIT by Ider and Birgul [4] for 2D problems. Also this method is applied for the 3D problems by Birgul at al [5]. In this work the conductivity distribution of the 3D object is calculated from the multi slice $\mathbf{B_z}$ measurements, at 5 different slices. However, constructing sensitivity matrix for 3D problems requires very long time and large memory in the computer. This is why the Sensitivity Matrix Method is not commonly used for 3D problems.

In order to improve the performance of the Sensitivity Matrix Method for 3D problems a method is suggested by Hamamura [6]. This method, assumes that the electrodes are placed on the whole length of the object in z direction and the conductivity distribution of the 3D object is z- invariant. Let's define $\mathbf{B}_{z\_2D}$ as the magnetic flux density distribution for a 2D object, and $\mathbf{B}_{z\_3D}$ as the magnetic flux density distribution which is calculated at the center slice of a 3D object. Let's assume that the conductivity distribution of the 3D object in x-y plane is equal to the conductivity distribution of the 2D object which lies in x-y plane and the conductivity distribution of the 3D object is z invariant. In this case, it is claimed that by using a Z correction factor, $\mathbf{B}_{z\_2D}$ can be transferred to the $\mathbf{B}_{z\_3D}$. Conversely, the $\mathbf{B}_{z\_3D}$ can also be transformed to the $\mathbf{B}_{z\_2D}$ using the Z correction factor. Therefore, if a $\mathbf{B}_{z\_3D}$ measurement is made at the center slice of the 3D object, this magnetic flux density can be converted to the $\mathbf{B}_{z\_2D}$ by a Z correction factor, as if this magnetic flux density arose from the 2D

object. Since $\mathbf{B}_{z\_2D}$ and $\mathbf{B}_{z\_3D}$ distributions can be converted to the each other by a Z correction factor, after measurement of the magnetic flux density from the 3D object, whole problem can be solved in 2D. This method reduces the time required to solve the conductivity distribution in an object. However, it is based on the assumption that the conductivity of the object is z invariant and the electrodes should run the whole length of the object . In practice, even the conductivity distribution inside an object is z invariant, using such a long electrode is impractical.

The performance of the MREIT algorithms also depends on the current density distribution inside the object. It is known that uniform internal current density distribution is desirable in order to obtain less noisy images. Song at al [7] designed a new electrode such that the uniform current distribution is achieved under the electrode surface. In this design, the thickness of the electrode is varying over the electrode in order to sustain a uniform current distribution under the surface of the electrode. The design is based on the assumption that conductivity distribution under the surface of the electrode is uniform. However, conductivity distribution may vary under the surface of the electrodes. In these cases the uniform conductivity distribution may not be achieved.

1.1 Objective and Scope of the Thesis

In Magnetic Resonance Electrical Impedance Tomography (MREIT), there are many algorithms to reconstruct conductivity distribution inside the object. One of these algorithms is the Sensitivity Matrix Method. However, this algorithm is not commonly used in 3D problems due to the fact that this method requires too much memory and time. Objective of this thesis is to investigate these limitations and bring solutions to them so that this algorithm can be used for solving 3D problems effectively.

The main limitation of this algorithm for 3D problems is that the construction of sensitivity matrix **D** takes too much time and the size of the constructed

sensitivity matrix $\mathbf{D}$ is too large. Due to the size of the $\mathbf{D}$ matrix, this algorithm necessitates large memory space. In this thesis, the object is divided into N finite element to solve the forward problem, and the calculation of the $\mathbf{D}$ matrix is made by changing each elements' conductivity to observe the change in the magnetic flux density at M measurement points. Therefore, the number of the required forward problem solution in order to construct the $\mathbf{D}$ matrix is equal to the number of the finite elements used to discretisize the object. Since there are many finite elements in a 3D object, the required calculations for the $\mathbf{D}$ matrix is time consuming. In this thesis, the calculation of the $\mathbf{D}$ matrix is simplified to decrease the time required to construct it. New calculated $\mathbf{D}$ matrix is called as the modified sensitivity matrix. Although the modified sensitivity matrix $\mathbf{D}$ is a modified version of the real one, conductivity distributions solved iteratively using these matrices, converge almost the same solution.

Another limitation of using a $\mathbf{D}$ matrix with a large size is that solving $\Delta\mathbf{B}_z = \mathbf{D}\Delta\boldsymbol{\sigma}$ for $\Delta\boldsymbol{\sigma}$ requires too much memory and time. In this thesis, an assumption is made for the elements of the $\Delta\boldsymbol{\sigma}$ vector, which results in reduction in the dimension of $\Delta\boldsymbol{\sigma}$ vector and so in the dimension of the $\mathbf{D}$ matrix. This reduction in the dimension of the $\mathbf{D}$ matrix not only reduces the memory space required to save $\mathbf{D}$ matrix but also results in reduction in the time required to solve $\Delta\mathbf{B}_z = \mathbf{D}\Delta\boldsymbol{\sigma}$ equation for reduced $\Delta\boldsymbol{\sigma}$ vector.

In the Sensitivity Matrix Method, it is necessary to calculate $\mathbf{B}_z$ (the z component of magnetic flux density) for a uniform conductivity distribution of the object. $\mathbf{B}_z$ is calculated for a uniform conductivity case at the measurement points of $\mathbf{B}_z$ measured by MRI. The difference between the calculated and measured $\mathbf{B}_z$, gives $\Delta\mathbf{B}_z$ which is the magnetic flux density arising from the difference of the conductivity of the object from the uniform conductivity. However, due to the fact that the model of the object cannot be constructed with exact boundaries, the calculated $\mathbf{B}_z$ becomes faulty. Therefore, $\Delta\mathbf{B}_z$ becomes

faulty. Also, inaccuracies in calculations and artifacts in measurements creates errors in $\mathbf{\Delta B_z}$. All of the errors mentioned above are dominant in the regions where the magnetic flux density changes rapidly. In this thesis, it is proposed that using a multichannel current source reduces these errors by producing uniform current distribution inside the object.

1.2 Outline of the Thesis

This thesis consists of five chapters. The second chapter discusses the Modified Sensitivity Matrix Method by comparing it with the Conventional Sensitivity Matrix Method. Boundary mismatches between the simulation object and the real object create errors on $\mathbf{\Delta B_z}$. In the third chapter, errors in $\mathbf{\Delta B_z}$ are investigated for different boundary mismatch cases. Then, in this chapter the use of the multichannel current source for the MREIT is discussed. The simulation and experimental methods and the results obtained by using these methods are given in each chapter to clarify the methods. Simulations and experiments based on the results of previous chapters are also given in the forth chapter. Finally, in the fifth chapter conclusions of the thesis are given.

Chapter 2 : Modified 3D Sensitivity Matrix Method

The Sensitivity Matrix Method is an algorithm to reconstruct the conductivity distribution inside the object. This method has usually been used for 2D problems. This is because of the fact that the calculation of the sensitivity matrix requires too much time. Also in 3D case the size of the sensitivity matrix becomes too large which may cause too long solution time and memory problem. The Modified 3D Sensitivity Matrix Method is developed in order to reduce the construction time of the sensitivity matrix, based on the Bz-Substitution MREIT algorithm suggested by Ider [8]. While Bz-Substitution MREIT was proposed for 2D problems, Modified 3D Sensitivity Matrix Method is proposed for 3D problems. Actually, both of these methods can be seen as a modified form of the Conventional Sensitivity Matrix Method. So, this chapter starts with explaining the algorithm of the Conventional Sensitivity Matrix Method and its disadvantages. After that, the advantages which come with the Modified Sensitivity Matrix Method, will be explained.

2.1 Conventional Sensitivity Matrix Method

After acquiring magnetic flux density data using a MRI system we need to reconstruct the conductivity of the object that we want to image. There are several conductivity reconstruction algorithms and one of them is the Conventional Sensitivity Matrix Method. This algorithm is an iterative algorithm to reconstruct electrical conductivity of an object from z component of the measured magnetic flux density. Algorithm consists of two main parts as forward and inverse problems.

2.1.1 Forward and Inverse Problems

Aim of the forward problem is to calculate the magnetic field produced by internal current distribution for known boundary and conductivity distribution.

On the other hand, calculation of conductivity distribution inside the object from the measured magnetic field is called inverse problem.

For solving the forward problem, the Finite Element Method can be used. For 3D case if we have a connected and bounded domain Ω in the xyz plane which is shown in Figure 2.1-a, with boundary Γ, unit outward normal along Γ, n, and positive non-zero conductivity σ, then potential field Φ in Ω should obey the Laplace's equation $\nabla.(\sigma\nabla\phi)=0$ in Ω. Also defining Neumann boundary condition $\sigma\frac{\partial\phi}{\partial n}=J_{app}$ on Γ, where J_{app} represents the injection pattern, we can solve Φ using FEM. Integral of J_{app} on Γ should be zero for the considered injection pattern.

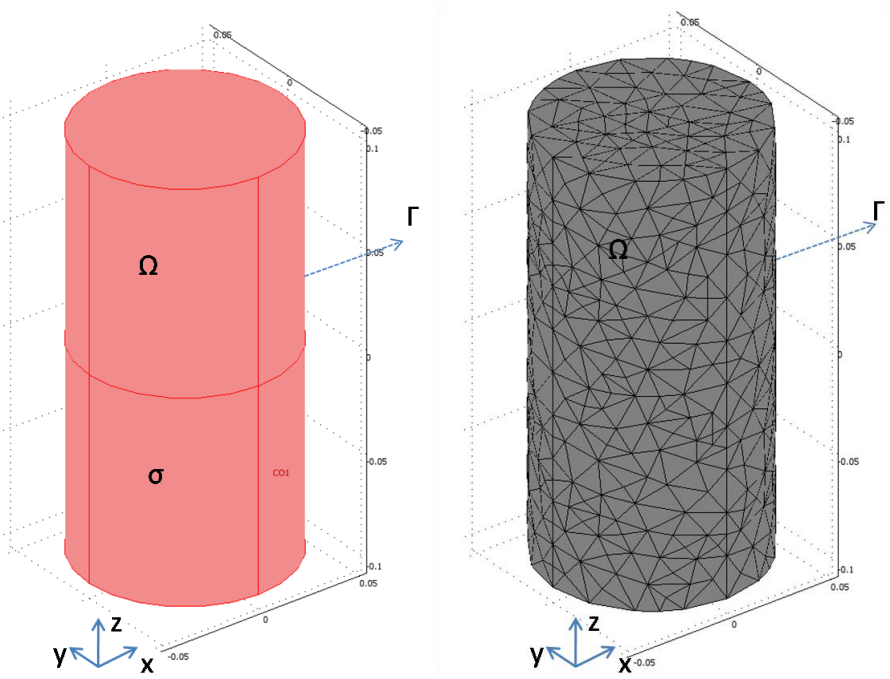

a b

Figure 2.1 (a) 3D object (b) 3D mesh of the object with tetrahedron finite elements

FEM necessitates to divide domain Ω into small finite elements, in order to solve potential field Φ. An example of mesh generated by dividing domain Ω into

N=34892 tetrahedron finite elements with n=6974 nodes given in Figure 2.1-b. If we use linear shape functions for finite elements and take conductivity constant inside each finite element we will have a conductivity value vector **σ=[** σ_1, σ_2, . . ., σ_N **]'** which has dimension Nx1 (34892x1). Using linear finite elements, FEM calculates the node potentials at the nodes of these finite elements. Because of the fact that we use linear shape functions for the finite elements, potential field at any point is assumed to vary linearly within each element. Thus potential field at any space point can be expressed as a linear combination of node potentials. Using boundary conditions and linear equations for each element, it is possible to write following equation:

$$\mathbf{A}(\sigma)\mathbf{\Phi} = \mathbf{b}$$

Here $\mathbf{A}(\sigma)$ is n by n coefficient matrix which is acquired from geometry and the conductivity distribution of the object, $\mathbf{\Phi}$ is a n by 1 vector which represents the unknown node potentials, and $\mathbf{b}$ is n by 1vector defining the boundary conditions on the nodes. Solving $\mathbf{A}(\sigma)\mathbf{\Phi} = \mathbf{b}$ equation for $\mathbf{\Phi}$ we can obtain potential values for each node. Using the equations $\mathbf{E} = -\nabla\mathbf{\Phi}$ and $\mathbf{J} = \boldsymbol{\sigma}\mathbf{E}$ it is possible calculate electric field and current density for each finite element. Since potential field linearly varies in each element, electric field and current density will be constant inside each element.

In order to calculate magnetic flux density Biot-Savart Law will be used. Biot-Savart Law relates the magnetic flux density to the current density as:

$$B_Z(x,y,z) = \frac{\mu_0}{4\Pi}\int_{\Omega} \frac{(y-y')\cdot J_X(x',y') - (x-x')\cdot J_Y(x',y')}{\left[(x-x')^2+(y-y')^2+(z-z')^2\right]^{\frac{3}{2}}} dx'dy'dz'$$

Since the current density is constant inside each finite element, it is possible to discretize this equation. Magnetic flux density of the jth node B_{z_j} at (x_j, y_j, z_j) . will be the sum of the magnetic flux densities at the jth node which are produced from the current densities of each element with center points (x_i, y_i, z_i) and volume V_i .

$$B_{z\,j} = \frac{\mu_0}{4\Pi} \sum_{i=1}^{N} \frac{(y_j - y_i) J_X(x_i, y_i) - (x_j - x_i) J_y(x_i, y_i)}{\left[(x_j - x_i)^2 + (y_j - y_i)^2 + (z_j - z_i)^2 \right]^{\frac{3}{2}}} V_i$$

Actually, by solving forward problem we want to calculate measured magnetic flux density by MRI. If we have acquired our MRI image at M nodes, our measured $\mathbf{B_z}$ vector will have a size Mx1, So the calculated $\mathbf{B_z}$ will also have Mx1 size. In order to calculate this $\mathbf{B_z}$ vector we can write a vector equation in the following form, using equation which is written for B_{z_j} :

$$\mathbf{B_z} = \mathbf{C_x J_x} + \mathbf{C_y J_y}$$

where $\mathbf{C_x}, \mathbf{C_y}$ are M x N matrices which depend only on the geometry and which are obtained from the discretized Biot Swart Law, and $\mathbf{J_x}, \mathbf{J_y}$ are Nx1 vectors containing the x and y components of current densitiy of each finite element. Since the current density of each element is equal to the electric field of that element times the conductivity of that element ($J_x(i) = E_x(i)\sigma(i)$ and $J_y(i) = E_y(i)\sigma(i)$) , we can write $\mathbf{J_x} = \mathbf{S_x}\boldsymbol{\sigma}$ and $\mathbf{J}_y = \mathbf{S}_y\boldsymbol{\sigma}$, by placing each of the electric field value of the i'th element to the i'th diagonal entry of N x N $\mathbf{S}$ matrix ($\mathbf{S_x(i,i) = E_x(i)}$ and $\mathbf{S}_y\mathbf{(i,i) = E}_y\mathbf{(i)}$). So $\mathbf{B_z}$ can be written in the following form:

$$\mathbf{B_z} = \mathbf{C_x S_x}\boldsymbol{\sigma} + \mathbf{C_y S_y}\boldsymbol{\sigma}$$

If we take this equation into the $\boldsymbol{\sigma}$ parenthesize and call $\mathbf{D}$ inside the parenthesize ($\mathbf{B_z} = (\mathbf{C_x S_x} + \mathbf{C_y S_y})\boldsymbol{\sigma}$) we will have an equation which is given below.

$$\mathbf{B_z} = \mathbf{D}\boldsymbol{\sigma}$$

In the conventional sensitivity matrix method as an inverse problem we have to find conductivity distribution $\boldsymbol{\sigma}$ from measured $\mathbf{B_z}$ according to the equation above. In this equation the only known is measured $\mathbf{B_z}$. Since $\mathbf{D}$ is a function of $\boldsymbol{\sigma}$ and it is desired to find $\boldsymbol{\sigma}$, an iterative solution can be used for finding $\boldsymbol{\sigma}$. The iterations start with assigning an initial conductivity distribution $\boldsymbol{\sigma}_0$ which

consists of an initial conductivity value for each finite element. If we change the initial conductivity distribution $\boldsymbol{\sigma}_0$ by $\Delta\boldsymbol{\sigma}$, the initial sensitivity matrix $\mathbf{D_0}$ will change as $\Delta\mathbf{D}$. So the new magnetic flux density will be in the following form:

$$\mathbf{B}_{z_{new}} = (\mathbf{D_0} + \Delta\mathbf{D})(\boldsymbol{\sigma}_0 + \Delta\boldsymbol{\sigma})$$

$$\mathbf{B}_{z_{new}} = \mathbf{D_0}\boldsymbol{\sigma}_0 + \mathbf{D_0}\Delta\boldsymbol{\sigma} + \Delta\mathbf{D}\boldsymbol{\sigma}_0 + \Delta\mathbf{D}\Delta\boldsymbol{\sigma}$$

In this equation $\Delta\mathbf{D}\Delta\boldsymbol{\sigma}$ can be ignored because its value is relatively small. So, the magnetic field difference $\Delta\mathbf{B}_z$ due to the change in conductivity vector by $\Delta\boldsymbol{\sigma}$ can be expressed as below.

$$\Delta\mathbf{B}_z = \mathbf{B}_{z_{new}} - \mathbf{D_0}\boldsymbol{\sigma}_0$$

$$\Delta\mathbf{B}_z = \mathbf{D_0}\Delta\boldsymbol{\sigma} + \Delta\mathbf{D}\boldsymbol{\sigma}_0$$

$$\Delta\mathbf{B}_z = \mathbf{D_0}\Delta\boldsymbol{\sigma} + \left.\frac{\partial(\mathbf{D}\boldsymbol{\sigma}_0)}{\partial\boldsymbol{\sigma}}\right|_{\boldsymbol{\sigma}_0}\Delta\boldsymbol{\sigma}$$

$$\Delta\mathbf{B}_z = \left(\mathbf{D_0} + \left.\frac{\partial(\mathbf{D}\boldsymbol{\sigma}_0)}{\partial\boldsymbol{\sigma}}\right|_{\boldsymbol{\sigma}_0}\right)\Delta\boldsymbol{\sigma}$$

In the above equation $\mathbf{D_C} = \left(\mathbf{D_0} + \left.\frac{\partial(\mathbf{D}\boldsymbol{\sigma}_0)}{\partial\boldsymbol{\sigma}}\right|_{\boldsymbol{\sigma}_0}\right)$ term is called as Conventional Sensitivity Matrix. In order to calculate $\mathbf{D_0}$, it is necessary to solve the forward problem just one time. On the other hand, the calculation of $\left.\frac{\partial(\mathbf{D}\boldsymbol{\sigma}_0)}{\partial\boldsymbol{\sigma}}\right|_{\boldsymbol{\sigma}_0}$ matrix requires solving the forward problem for conductivity change at each finite element (The derivation of the term $\left.\frac{\partial(\mathbf{D}\boldsymbol{\sigma}_0)}{\partial\boldsymbol{\sigma}}\right|_{\boldsymbol{\sigma}_0}$ is given in Appendix A.). This means that in order to calculate $\left.\frac{\partial(\mathbf{D}\boldsymbol{\sigma}_0)}{\partial\boldsymbol{\sigma}}\right|_{\boldsymbol{\sigma}_0}$, it is necessary to solve the forward problem N times. Since solving the forward problem N times requires too much time, the Modified Sensitivity Matrix Method is suggested in this thesis.

2.1.2 Algorithm of Conventional Sensitivity Matrix Method

1. Divide the object into finite elements.
2. Assign an initial conductivity value to each element. $\boldsymbol{\sigma}_0$ vector contains the all initial conductivity values for all elements. The conductivity values of all the elements are usually chosen as the same value so that the conductivity distribution inside the object is uniform.
3. Solve forward problem using initial conductivity distribution $\boldsymbol{\sigma}_0$ to calculate $\mathbf{B_z}$ and $\mathbf{D}_0$.
4. Subtract calculated $\mathbf{B_z}$ from measured $\mathbf{B_z}$, to find $\Delta\mathbf{B_z}$.
5. By solving forward problem it is possible to solve the change in electric field due to the change in the conductivity of an element. Solve forward problem N times to calculate conventional sensitivity matrix $\mathbf{D_C}$.
6. Solve $\Delta\mathbf{B_z} = \mathbf{D_C}\Delta\boldsymbol{\sigma}$ to find the change in conductivity $\Delta\boldsymbol{\sigma}$.
7. Add the change in conductivity $\Delta\boldsymbol{\sigma}$ to initial conductivity $\boldsymbol{\sigma}_0$. $(\boldsymbol{\sigma}_N = \boldsymbol{\sigma}_0 + \Delta\boldsymbol{\sigma})$
8. Solve forward problem to find new $\mathbf{B_z}$ and $\mathbf{D}_0$ for $\boldsymbol{\sigma}_N$.
9. Subtract new calculated $\mathbf{B_z}$ from measured $\mathbf{B_z}$, to find new $\Delta\mathbf{B_z}$.
10. If new $\Delta\mathbf{B_z}$ is small enough, stop iterations. Otherwise, continue iterations from 5th step by assigning $\boldsymbol{\sigma}_0 = \boldsymbol{\sigma}_N$.

2.2 Modified Sensitivity Matrix Method

The calculation of the term $\left.\frac{\partial(\mathbf{D}\boldsymbol{\sigma}_\mathbf{0})}{\partial\boldsymbol{\sigma}}\right|_{\boldsymbol{\sigma}_0}$ in the Conventional Sensitivity Matrix Method, requires too much time. So in the Modified Sensitivity Matrix Method, this term is not calculated and ignoring this term $\Delta\mathbf{B_z} \approx \mathbf{D}_0\Delta\boldsymbol{\sigma}$ can be written. By simulations it will be shown that, the Conventional and Modified Sensitivity Matrix Methods will converge to similar solutions.

2.2.1 Algorithm of Modified Sensitivity Matrix Method

1. Divide the object into finite elements
2. Assign an initial conductivity value to each element. $\boldsymbol{\sigma}_0$ vector contains the all initial conductivity values for all elements. The conductivity values of all the elements are usually chosen as the same value so that the conductivity distribution inside the object is uniform.
3. Solve the forward problem by using the initial conductivity distribution $\boldsymbol{\sigma}_0$ to calculate $\mathbf{B_z}$ and $\mathbf{D}_0$.
4. Subtract calculated $\mathbf{B_z}$ from measured $\mathbf{B_z}$, to find $\Delta\mathbf{B_z}$.
5. Solve $\Delta\mathbf{B_z} = \mathbf{D}_0\Delta\boldsymbol{\sigma}$ to find the change in the conductivity ($\Delta\boldsymbol{\sigma}$).
6. Add the change in conductivity $\Delta\boldsymbol{\sigma}$ to the initial conductivity $\boldsymbol{\sigma}_0$. ($\boldsymbol{\sigma}_N = \boldsymbol{\sigma}_0 + \Delta\boldsymbol{\sigma}$)
7. Solve the forward problem to find new $\mathbf{B_z}$ and $\mathbf{D}_0$ for $\boldsymbol{\sigma}_N$.
8. Subtract the new calculated $\mathbf{B_z}$ from measured $\mathbf{B_z}$, to find the new $\Delta\mathbf{B_z}$.
9. If the new $\Delta\mathbf{B_z}$ is small enough, stop iterations. Otherwise, continue iterations from 5th step by assigning $\boldsymbol{\sigma}_0 = \boldsymbol{\sigma}_N$.

2.3 Simulation Results

In order to simulate the Conventional and Modified Sensitivity Matrix Methods, a cylindrical phantom given in Figure 2.2-a with diameter 10cm and height 20cm is used. The 3D mesh of the simulation phantom is given in the Figure 2.2-b. This mesh consists of 31 layers and each layer consists of 1126 triangular prisms. Also, in order to solve the forward problem, each triangular prism elements are divided into 3 tetrahedron finite elements as shown in Figure 2.2-b Two objects with 1.5 cm and 3cm diameter and 4.5 cm height are placed inside the phantom to form regions which have different conductivity values. The positions of the objects inside the phantom and the conductivity distribution at

the center slice is given in Figure 2.3. Magnetic field is calculated at the center axial slice of this phantom. Since magnetic field is related to magnetic flux density by a magnetic permeability constant, both of these are used in simulations throughout the thesis.

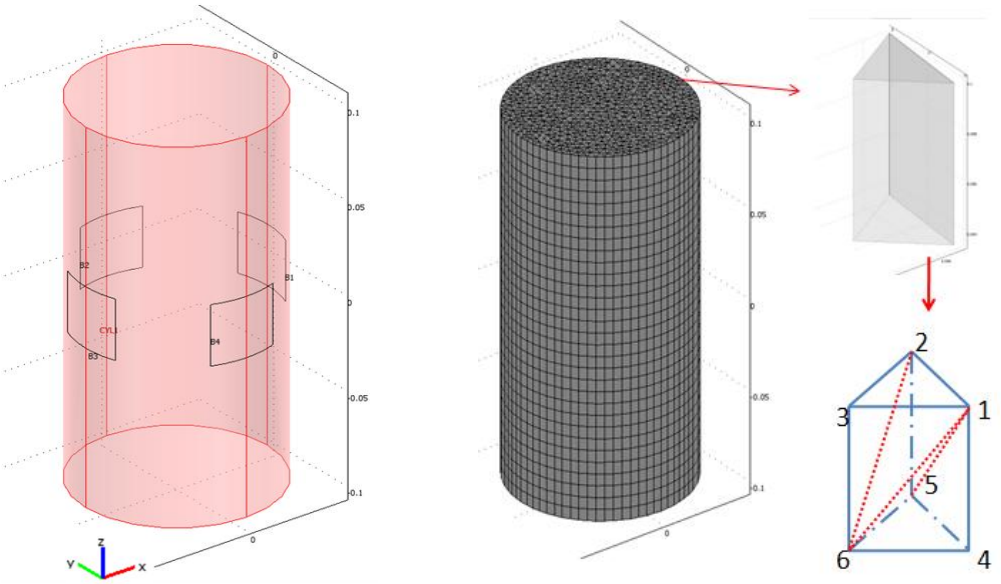

a) b)

Figure 2.2 a) Cylindrical simulation phantom b) Mesh of the cylindrical simulation phantom

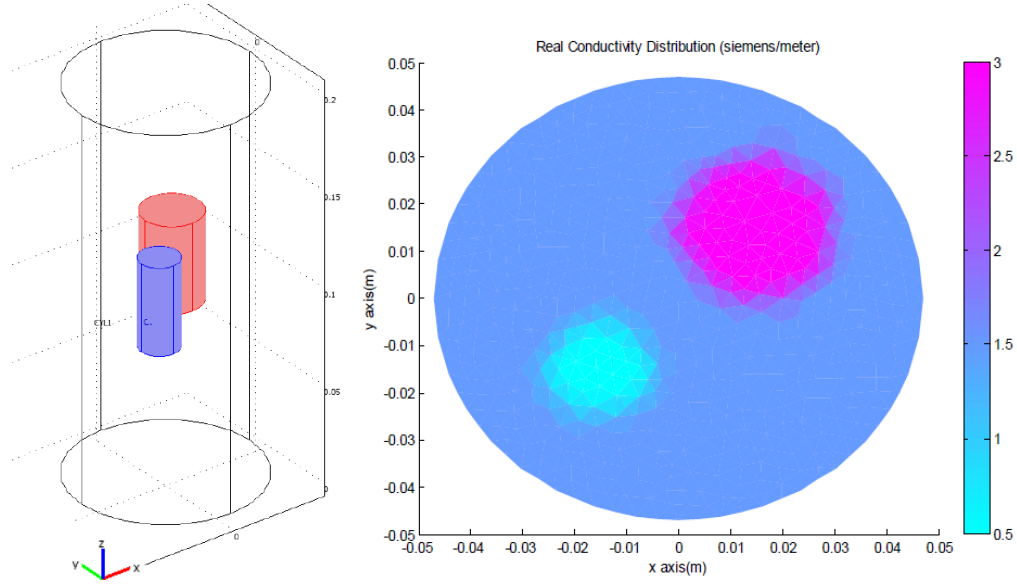

Figure 2.3 a) Position of the objects placed in to the phantom simulation phantom b)The real conductivity distribution at the center slice of the phantom

2.3.1 Sensitivity Analysis in z-direction

The sensitivity of the magnetic field to the conductivity of an element can be defined as the change in magnetic field due to the change in conductivity of that element. In Figure 2.4 the sensitivity of the center slice magnetic field to an element which is located in the center slice is given.

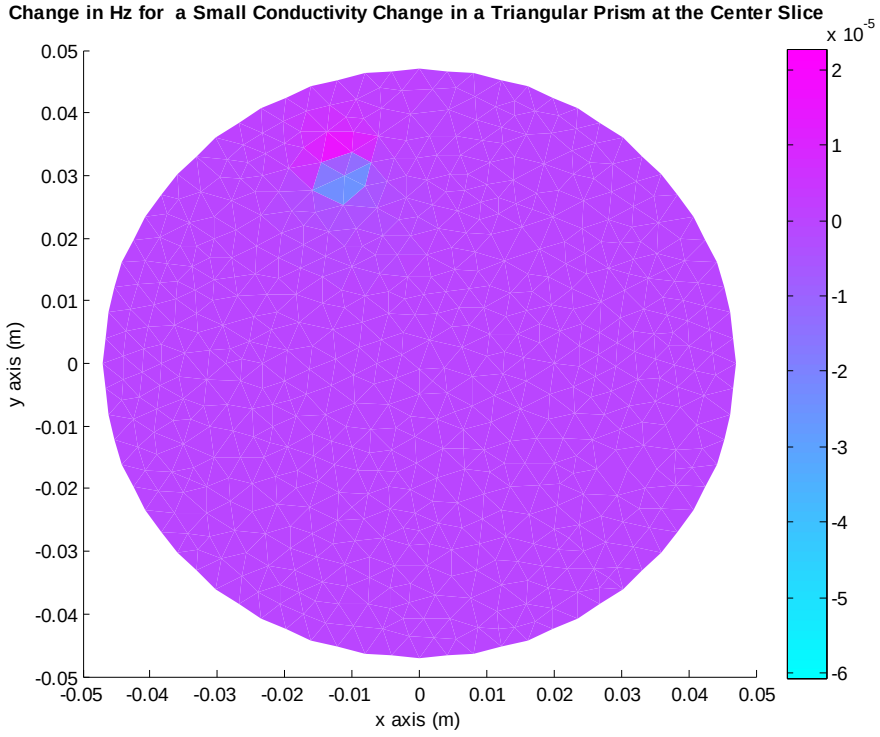

Figure 2.4 The sensitivity of the center slice magnetic field to an element which is located in the center slice is given

It is desired to investigate how the sensitivity of the center slice magnetic field depends on the conductivity of an element as the distance of the element to the center slice is varied. For this purpose the conductivity of elements on a vertical line are changed one by one and for each element $\mathbf{\Delta H_z}$ is calculated. Then, the maximum value of $\mathbf{\Delta H_z}$ is calculated. Finally, maximum of $|\mathbf{\Delta H_z}|$ values are plotted for each element with respect to the distance of the elements to the center slice.

From the plot in Figure 2.5 it is seen that if the distance of the element to the center slice is zero, the sensitivity of the center slice magnetic field to the change in the conductivity of the element is maximum. Although the sensitivity of the center slice magnetic field to the elements in the ± 2 layer range still remains significant, the sensitivity of the center slice magnetic field to the elements' conductivity becomes negligible after 2 layers distance. Therefore, assumptions for conductivity of the elements which are away from the center slice, do not change calculated magnetic field at the center slice significantly. Our assumption is that conductivity is not changing in the z direction. It is assumed that the triangular prisms which are in the same x, y coordinates have the same conductivity values. With this assumption, three dimensional problem is reduced to two dimensional form which results in reduction in the number of unknown from 34906 to 1126. Here 34906 is the total number of prisms and 1126 is the number of prisms in each layer.

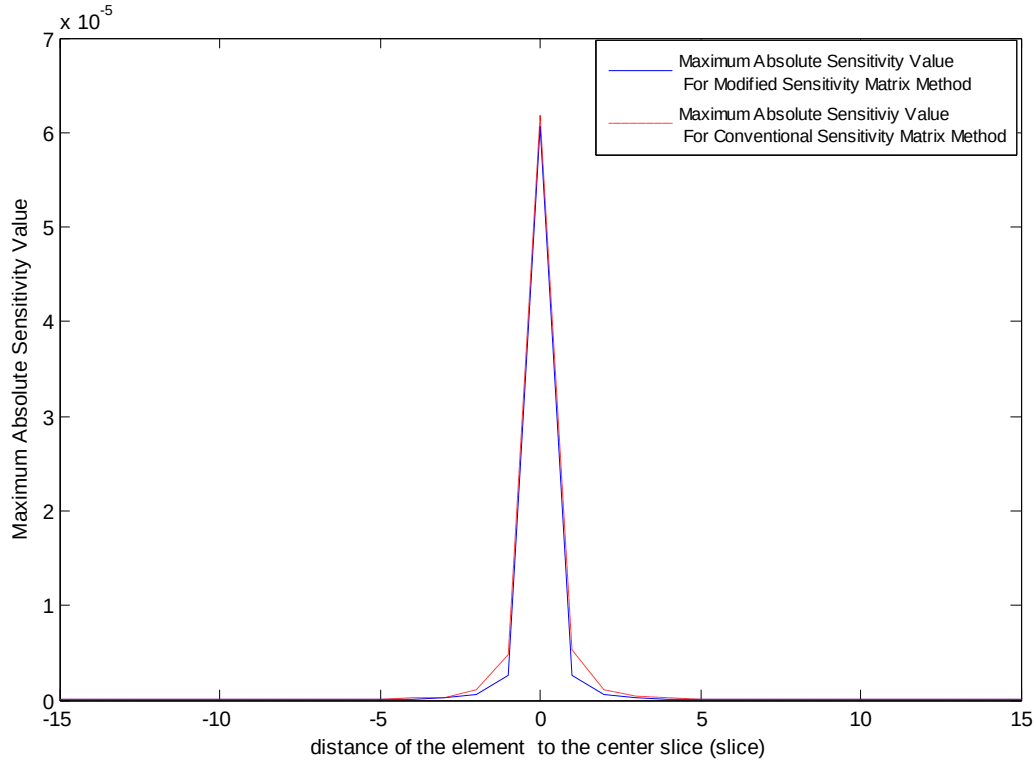

Figure 2.5 Distance of the element to the center slice of the phantom (slice) versus the maximum absolute sensitivity value of the center slice magnetic field to the element.

2.3.2 Comparison of the Conventional Sensitivity Matrix Method with the Modified Sensitivity Matrix Method

For simulations, the forward 3D problem for the real conductivity distribution is solved to find Hz. And a Gaussian noise is added to the acquired magnetic field to represent noise which might be accumulated due to the MRI system. For the conventional sensitivity matrix method after three iterations conductivity distribution at the center slice of the phantom is found with %4.09 error percentage. Found conductivity distribution after each iteration step are shown in Figure 2.6. These three iterations take 39 minutes.

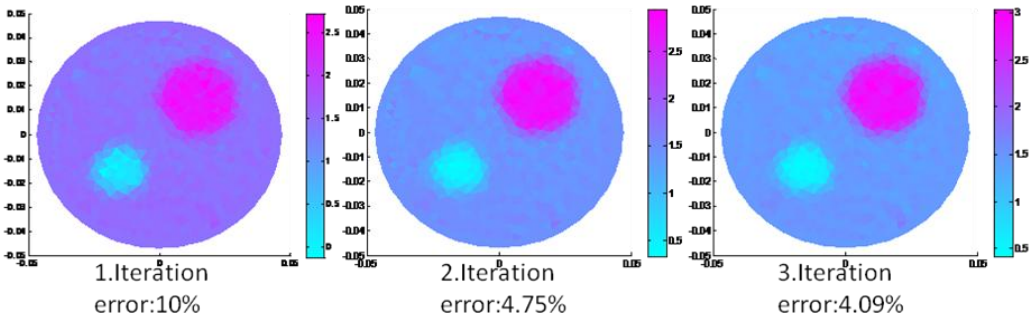

Figure 2.6 Conductivity distributions acquired using the Conventional Sensitivity Matrix Method for the three iteration

Convergence of the conductivity distribution and magnetic field versus iteration number for the Conventional Sensitivity Matrix Method is given in Figure 2.7.

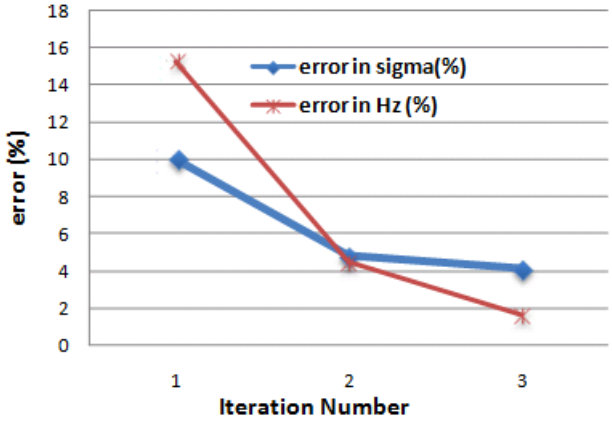

Figure 2.7 Convergence of the conductivity distribution and magnetic field versus iteration number for the conventional sensitivity matrix method

On the other hand, using the Modified Sensitivity Matrix Method it is possible to reconstruct conductivity distribution with the same error percentage (%4.59) within 1.3 minutes. Conductivity distribution acquired at the center slice of the phantom for three of the five iteration steps are shown in Figure 2.8.

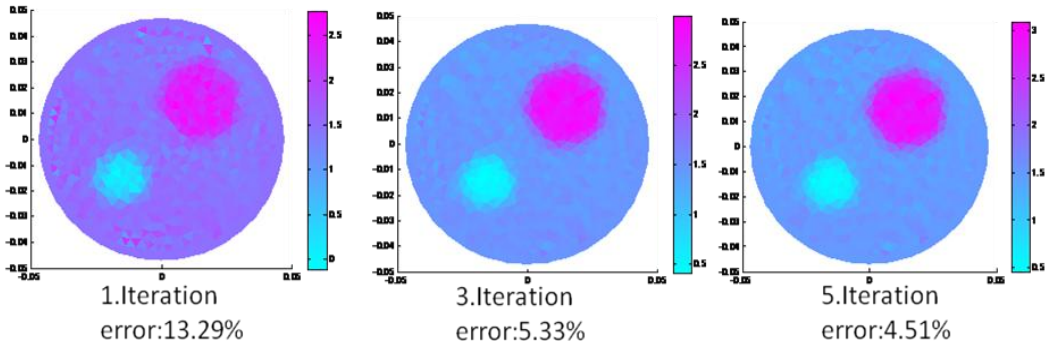

Figure 2.8 Conductivity distributions acquired using the Modified Sensitivity Matrix Method for the three iterations (1,3 and 5. iterations)

Convergence of the conductivity distribution and magnetic field versus iteration number for the Modified Sensitivity Matrix Method is given in Figure 2.9.

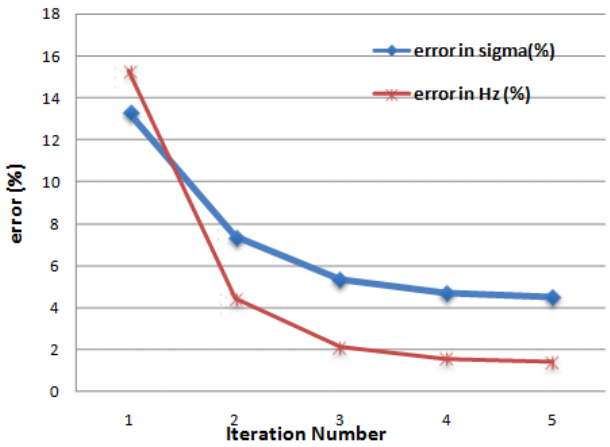

Figure 2.9 Convergence of the conductivity distribution and magnetic field versus iteration number for the modified sensitivity matrix method

In general, the Conventional Sensitivity Matrix Method requires about three iterations to converge a solution. On the other hand, the Modified Sensitivity Matrix Method requires from five to ten iterations to converge the same

solution. However, the Modified Sensitivity Matrix Method still necessitates less time than the conventional one. This is because of the fact that each iteration of the Modified Sensitivity Matrix Method takes significantly less time than the conventional one.

Chapter 3 : Multichannel Current Source for MREIT

In MREIT, the use of uniform internal current distribution is important in order to reconstruct less noisy conductivity distributions. However, uniform current distribution cannot be obtained by using a classical single channel current source. Also, using single channel current source results in sudden magnetic flux density changes around the electrodes. Measurements of magnetic flux density have artifacts due to this sudden changes in the magnetic flux density. Also, it is more likely to observe errors in calculation of the magnetic flux density around the regions where the magnetic flux density changes rapidly. Another problem with using the single channel current source is that calculated ΔB_z might be more sensitive to geometry errors made in the simulation which is used to calculate magnetic flux density for the uniform conductivity distribution. In this thesis, the use of the multichannel current source is proposed in order to reduce the errors in ΔB_z which are arising from the geometry mismatches, measurement artifacts and inaccuracies in calculations. The use of the multichannel current source reduces these errors by producing a nearly uniform current distribution even around the electrodes.

3.1 Effects of Errors in Boundary and Electrode Positions to the Difference Magnetic Field ΔB_z

As mentioned earlier in the algorithms of the Conventional Sensitivity Matrix Method and the Modified Sensitivity Matrix Method, the Sensitivity Matrix Method requires to subtract calculated magnetic flux density B_z from the measured one. The success of the sensitivity matrix algorithm depends on the correctness of the calculation of ΔB_z. If the initial conductivity assumption is subtracted from the real conductivity distribution, the difference should generate ΔB_z. However, if the boundary of the simulation object is different than the real objects' boundary, in ΔB_z also a difference occurs due to this boundary mismatch. This is because of the fact that for different geometry profiles there are

different types of current profiles, and these different current profiles create different magnetic flux density distributions. Therefore, these boundary mismatches cause ΔB_z distribution whose values are different than zero. Since ΔB_z is not correct, the calculated conductivity values are also faulty. In order to minimize these faults, the effects of the certain boundary mismatches are investigated. This work consists of solving the forward problem for several possible boundary mismatch cases and calculating resulting error on ΔB_z. For simulations a cylindrical phantom with recessed electrode regions is used. In Figure 3.1-a the simulation phantom is shown with its recessed parts (pink shows recessed electrode regions). Also, the electrodes are shown on the recessed region with circles. Errors in ΔB_z are calculated at the circler region of the center slice which is shown at Figure 3.1-b.

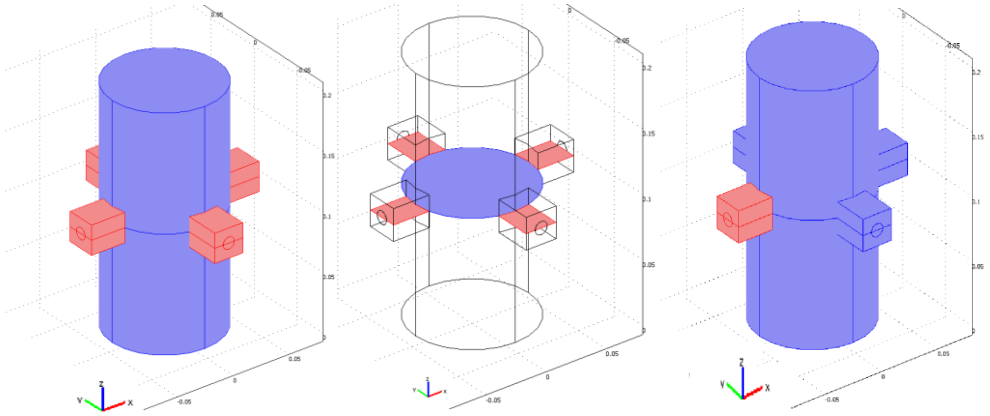

a. b. c.

Figure 3.1 a) Simulation phantom with recess electrode parts b) Center slice of the simulation phantom c) Selected recess part of the phantom

In order to calculate boundary mismatch effects on ΔB_z, B_z is calculated at the center slice of a phantom with uniform conductivity distribution. This phantom represents the real conductivity distribution and real boundary condition. So, the calculated B_z is assigned as the real magnetic flux density at the center slice of this phantom. The maximum absolute value of this B_z distribution is found as 116.3 nT. In order to simulate boundary mismatch cases, for each case the geometry of the phantom is changed and a new B_z distribution is calculated.

Afterwards, subtracting the new $\mathbf{B}_z$ from the real one and taking its absolute value $|\Delta \mathbf{B}_z|$ is calculated. Maximum values of $|\Delta \mathbf{B}_z|$ for each case are shown in Table 3.1. In order to clarify defined cases in Table 3.1, the 1mm shift of selected recessed part towards +y direction is shown in Figure 3.2 (Selected recessed part of the phantom is shown in Figure 3.1-c with pink color.).

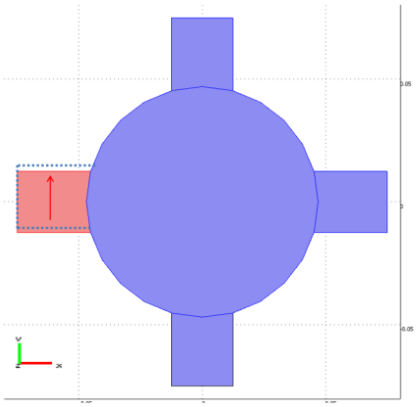

Figure 3.2 "1 mm" shift of the selected recess part towards to +y direction

Case Number	Case	maximum |ΔBz |(nT)	maximum |Bz| (nT)
1	Initial (real) case		116.3
2	Selected recessed part is 1mm shifted towards +y direction.	17.25	114.9
3	Selected recessed part is 1mm shifted towards -y direction.	17.33	117.5
4	Width of the selected recessed part is 1mm narrowed without changing its center of gravity.	12.29	119.5
5	Height of the selected recessed part is 1mm narrowed.	0.99	115.9
6	Electrode over the selected recessed part is 2mm shifted towards +z direction.	2.1	118.2
7	Electrode over the selected recessed part is 1mm shifted towards +y direction.	1.73	117.7
8	Phantom is modeled 3cm longer in +z direction.	0.71	116.2
9	$\mathbf{B}_z$ is calculated 1mm above (in z direction) the center slice.	0.74	116.2
10	$\mathbf{B}_z$ is calculated from average of 5 different slice at the center of the z direction with 1mm slice thickness.	0.74	118.8

Table 3.1 Errors in $\Delta \mathbf{B}_z$ due to the wrong definition of the boundary positions

From Table 3.1 it is seen that the errors made at the intersection of the cylindrical part of the phantom with the recess part, create more errors in the

calculation of $\mathbf{B}_z$. According to the results which are shown in Table 3.1 other geometry mismatches do not have significant effects on the error in $\mathbf{B}_z$. However, the intersections of the recess parts with the cylindrical part represents the electrode positions when there is no recess part for the electrodes. So, if there is no recess part, the errors in the position of the electrodes cause high $\Delta\mathbf{B}_z$ errors around the electrode region.

3.2 Known Problems with Single Channel Current Source in MREIT

As mentioned earlier in order to create magnetic flux density inside the imaging object, it is needed to inject current into the object. However, the current injection profile which uses a single electrode pair to inject current into an object have some problems. First of all, uniform current distribution which is preferable for MREIT applications, cannot be obtained using this current injection profile. Secondly, due to the single electrode pair profile, the boundary mismatches especially around the electrodes produce high errors in $\Delta\mathbf{B}_z$,which is important for the algorithms running based on $\Delta\mathbf{B}_z$. Also, the rapid changes in $\mathbf{B}_z$ around the electrode cause high errors in Laplace of the $\mathbf{B}_z$. These errors affect the algorithms which are using Laplace of the $\mathbf{B}_z$. Finally, the applied current to the electrodes is not distributed uniformly over the electrode, instead most of the current is injected around the edges of the electrodes.

Some of the MREIT reconstruction algorithms use measured current distribution in order to reconstruct conductivity distribution. For these algorithms the magnitude of the current holds a critical role. Found conductivity values are not reliable in the regions where the magnitude of the current is low. Due to the fact that the current distribution inside the object cannot be controlled with known current injection profiles, it is likely to observe that some regions inside the object have low current density distribution. For these regions calculated conductivity values are not reliable.

Injecting current into the object through small flat electrodes is the worst case of using a single electrode pair. In this case, current density is concentrated around the electrodes, which leads to a current density profile which is far away from being uniform. In order to sustain uniform current distribution for the region of interest, it might be useful to use larger electrodes which are large enough to cover the boundary of the region of interest. However, injected current through the surface of the electrodes are not constant over the surface of the electrodes. Most of the current is injected from the edges of the electrodes. So, injected current is still not uniform even near the electrode surface. A uniform current density electrode is proposed by Song at al [7] to ensure uniform current distribution over the surface of the electrode. However, current profile over the surface of electrode is also determined by the conductivity distribution under the electrode. In other words, current distribution over the surface of the electrode can be uniform when the conductivity distribution under the electrode is uniform. As mentioned above, it is preferable to have uniform current distribution around the region of interest which cannot always be sustained by uniform current electrodes. This is because of the fact that current distribution inside the object depends on not only the current distribution over the surface of the electrode but also the geometry of the object, and the conductivity distribution inside the object. So, even with uniform current density electrodes it might not be possible to generate a uniform current distribution inside the object.

Also, some of the MREIT algorithms directly reconstruct conductivity distribution from z component of the measured magnetic flux density ($\mathbf{B}_z$). Among these algorithms some of them require solving the magnetic field intensity for known boundary and an initial conductivity distribution assumption. The next step in these algorithms, is subtracting the simulated $\mathbf{B}_z$ from the $\mathbf{B}_z$ measured by MRI system. If one electrode pair is used to inject

current into the object, there might be too much difference in $\Delta \mathbf{B}_z$ around the electrodes. Since $\mathbf{B}_z$ magnitude is very high and very variable around the electrodes, these regions are too sensitive to any boundary mismatch.

As mentioned earlier if the current is applied from a classical single electrode pair, current density is concentrated around specific regions, which leads to a rapid change in current density around these regions. This rapid change in current results in rapid change in $\mathbf{B}_z$, which causes more errors around the electrodes with respect to the other regions in Laplace of $\mathbf{B}_z$.

3.3 Using Multichannel Current Source in MREIT

In order to solve the problems occurring due to the single electrode pair current injection profile, the use of a multichannel current source is suggested. Using multiple electrode pairs (channel) to inject current into the object, allows to control current distribution inside the object that we want to image. On the other hand, if the current is applied from a single electrode pair, it is not possible to control current distribution inside the object. Some of the MREIT algorithms reconstruct the conductivity values from the current distribution. These algorithms are not reliable for the regions where the current density is low. Therefore, it is crucial to control current distribution inside the object. Also, by using multichannel current injection profile, it is possible to distribute total current among many electrodes. When the current is distributed among many electrodes, magnitude of $\mathbf{B}_z$ around the electrodes is low. But it is higher when the total current is injected through one electrode pair. Algorithms requiring subtracting simulated $\mathbf{B}_z$ from the measured $\mathbf{B}_z$, are more sensitive to boundary definition errors for the regions where $\mathbf{B}_z$ magnitude changes rapidly. So, injecting current through multiple electrodes decreases the algorithms' sensitivity to boundary mismatches between the simulation and reality.

3.4 Experiment: investigation of the effect of the multi channel current source on $\Delta \mathbf{B_z}$

3.4.1 Acquisition of the z component of the magnetic flux density ($\mathbf{B_z}$)

In the experiments, the standard spin-echo pulse sequence (Figure 3.3) is used to acquire MRI images. In order to acquire a $\mathbf{B_z}$ distribution at a slice which arise from the current injection, two MRI images are acquired at that slice. For these two acquisitions, currents of opposite polarities (I(+), I(-)) are applied for a total duration of T_c. In Figure 3.3, spin echo pulse sequence and the current waveforms of I(+) and I(-) for two acquisitions are shown. As a result of these current injections, the acquired images take the form below:

$$M^{\pm}(x,y) = m(x,y)\exp(j\delta(x,y))\exp(\pm j\gamma \mathbf{B_z}(x,y)T_c)$$

Here $m(x,y)$ is the transverse magnetization, $\delta(x,y)$ is the systematic phase artifact, γ is the gyromagnetic ratio, and $\mathbf{B_z}$ is the magnetic flux density which arises from the current injection. The phases of these two images are given below in radians.

$$\Phi_1 = \delta(x,y) + \gamma \mathbf{B_z}(x,y)T_c$$

$$\Phi_2 = \delta(x,y) - \gamma \mathbf{B_z}(x,y)T_c$$

From these two phases $\mathbf{B_z}$ can be calculated as $\mathbf{B_z}(x,y) = (\Phi_1 - \Phi_2)/(2\gamma T_c)$. Other MRI imaging parameters are given in each experimental procedure.

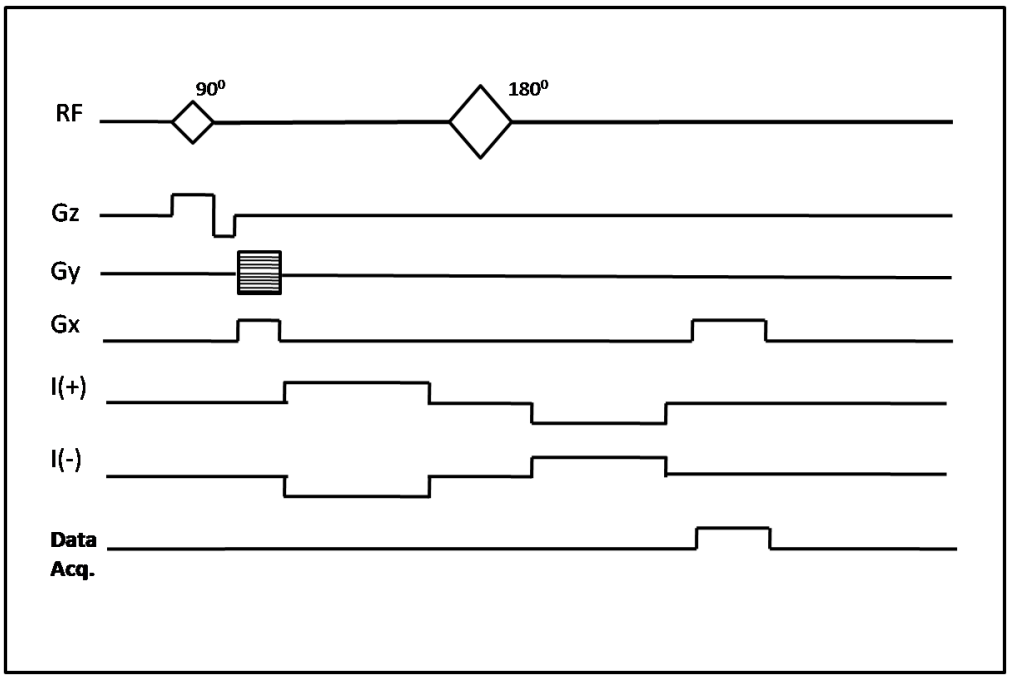

Figure 3.3 Spin echo pulse sequence and current injections for positive and negative directions.

3.4.2 Experimental procedure and results

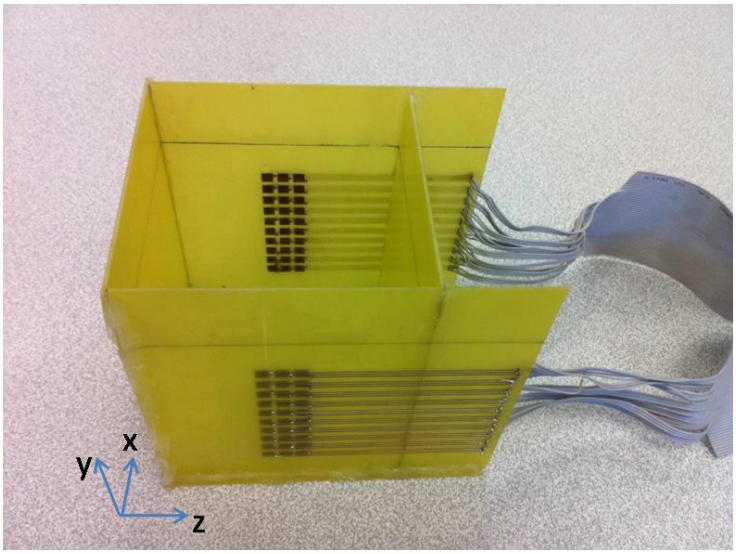

Figure 3.4 Cubic phantom with multiple electrodes

Two experiments are conducted to show that multichannel current source reduces the errors in $\mathbf{\Delta B}_z$ due to boundary mismatches, inaccuracies in the

calculation of magnetic flux density for a uniform case and measurement artifacts. In the first case, the current is injected into the object through six electrode pairs while in the second case, the current is injected into the object through thirty electrode pairs. In both of the experiments a cubic phantom shown in Figure 3.4 filled with 12gr/L agar, 12gr/L NaCl, 1gr/L $CuSO_4$ and distilled water is used. As an object, a plastic balloon filled with 12gr/L NaCl, 1gr/L $CuSO_4$ and distilled water is used. Since the plastic balloon is not conductive, the phantom consists of highly conductive and insulating conductivity regions. These regions are shown in Figure 3.5 on the MRI magnitude image. MRI parameters are chosen as TR: 900 ms, TE: 60 ms, T_c= 42 ms, FOV: 150 mm, Resolution: 256*256, Slice Thickness: 5 mm. In the first experiment 19mA total current is injected through the six electrode pairs shown at the top left of the Figure 3.6. From each electrode pair the same amount of current is injected into the object which is around 3.17mA. At the top right of the Figure 3.6 the z component of the magnetic flux density ($\mathbf{B}_z$) distribution acquired from MRI system for six electrode current injection profile is shown. $\mathbf{B}_z$ distribution is calculated for the uniform conductivity distribution and six electrode current injection profile. This $\mathbf{B}_z$ distribution is shown at the bottom-left of the Figure 3.6. If we subtract $\mathbf{B}_z$ acquired in the experiment, from the $\mathbf{B}_z$ calculated at the simulation, $\Delta\mathbf{B}_z$ is obtained at the bottom left of the Figure 3.6. As expected, a $\mathbf{B}_z$ difference can be observed around the object due to its conductivity difference. However, around the electrodes, there are unexpected $\mathbf{B}_z$ differences due to the mismatches of the electrode positions. In the second experiment, the same amount of the total current (19mA) is injected in to the object from thirty electrode pairs which are shown at the top left of the Figure 3.6. From each electrode pair the same amount of current is injected to the object which is around 0.63mA per channel. In this case $\mathbf{B}_z$ acquired from MRI, and $\mathbf{B}_z$ calculated from the simulation for a uniform case are shown at the top right and the bottom right of the Figure 3.7 respectively. The difference

magnetic flux density $\Delta \mathbf{B}_z$ calculated in this part of experiment is shown at the bottom left of the Figure 3.7. As expected, there is a difference in $\Delta \mathbf{B}_z$ around the object due to the difference of the conductivity of the object. As opposed to the first part of the experiment, there is no $\mathbf{B}_z$ difference around the electrodes. So we can conclude that the multichannel current source reduces the errors around the electrode region due to the boundary mismatches, calculation inaccuracies and measurement artifacts.

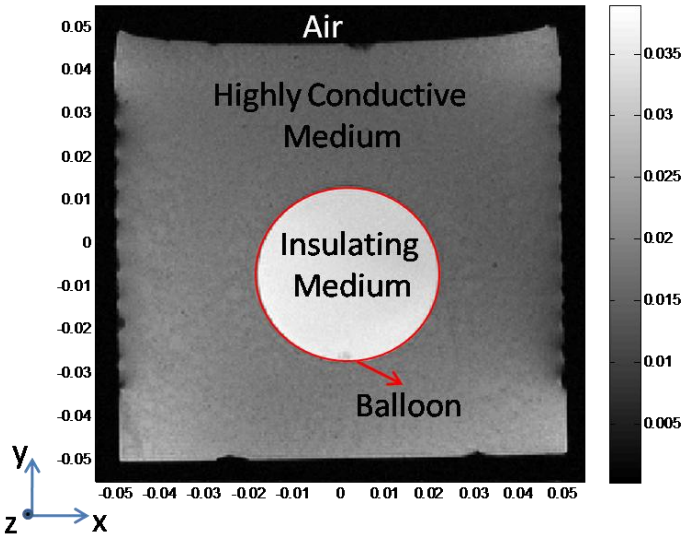

Figure 3.5 Conductivity distribution inside the phantom on the MRI magnitude image

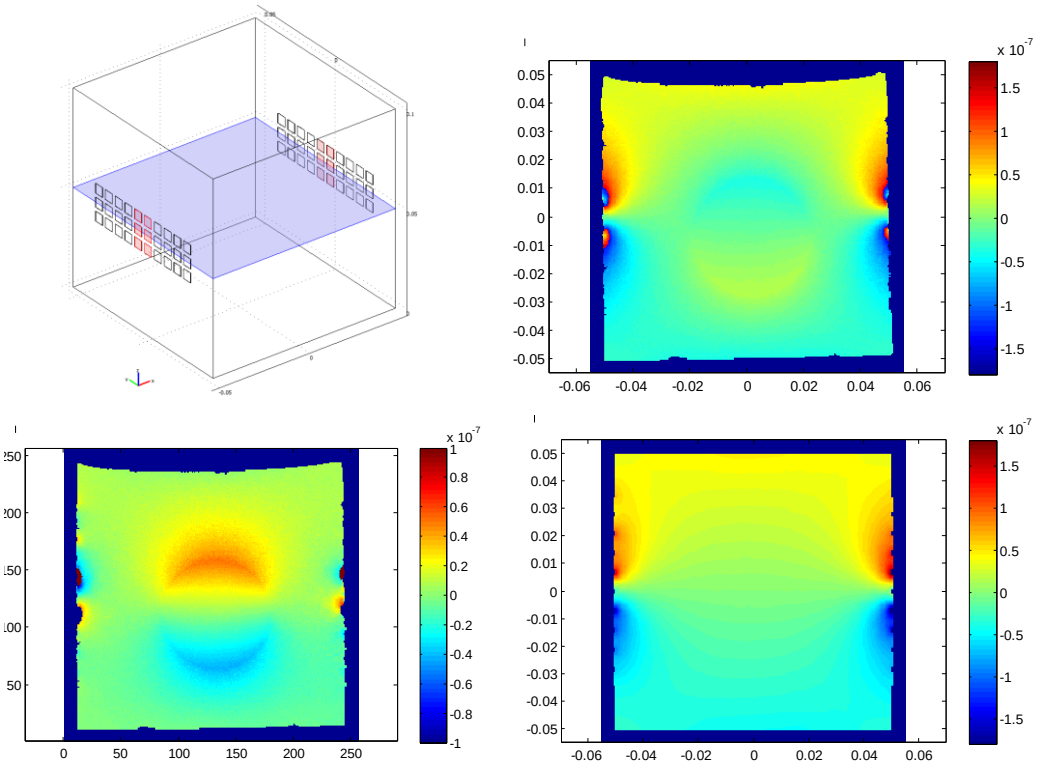

Figure 3.6 Electrodes used to inject current into the object and imaging slice (Top Left) The magnetic flux density difference acquired for the six electrode current injection profile. (Bottom Left) The magnetic flux density measured for the six electrode current injection profile (Top Right) The magnetic flux density calculated for the six electrode current injection profile and uniform conductivity distribution (Bottom Right)

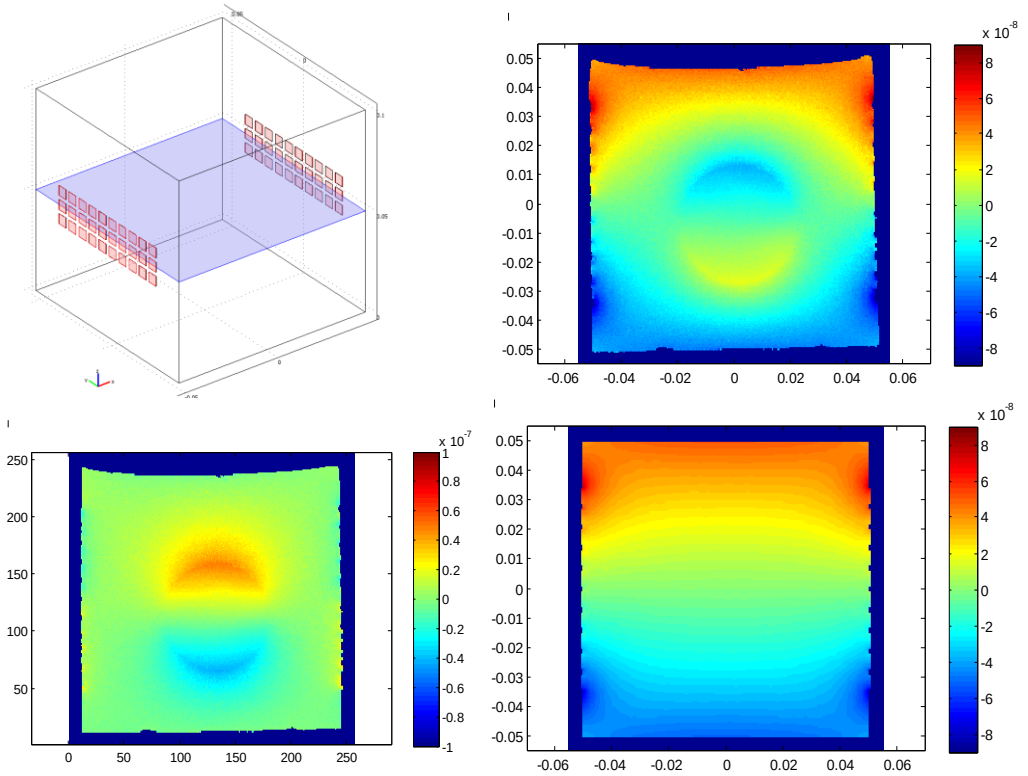

Figure 3.7 Electrodes used to inject current into the object and imaging slice (Top Left) The magnetic flux density difference acquired for the multiple (30) electrode current injection profile. (Bottom Left) The magnetic flux density measured for the multiple (30) electrode current injection profile (Top Right) The magnetic flux density calculated for the multiple (30) electrode current injection profile and uniform conductivity distribution (Bottom Right)

Chapter 4 : Simulation and Experimental Results For Conductivity Reconstruction

4.1 Simulation Results of Conductivity Reconstruction for 3D object

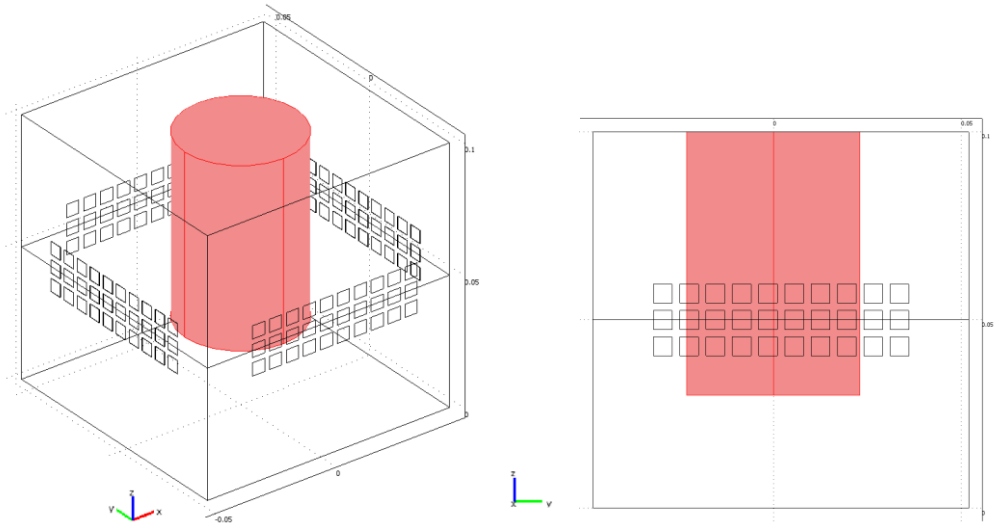

a) b)

Figure 4.1 a) Simulation phantom b) z-y cross section of the phantom

A cubic phantom with dimensions 10 cm is used as the simulation phantom. (Figure 4.1). A cylindrical object with diameter 4.8cm and height 7cm is placed into the phantom as shown in Figure 4.1. Conductivity of the object is chosen as 0.71 S/m and the background of the phantom is chosen as 1.76 S/m. In simulations the Sensitivity Matrix Method is used to reconstruct conductivity distribution. Magnetic flux density distribution is calculated at 13 slices. There is a 7mm gap between two consecutive slices. These 13 slices where the magnetic flux density is calculated are shown in Figure 4.2. In the first case, conductivity distribution in 5 different regions is reconstructed from the magnetic flux density distribution which is calculated at 13 different slices. The

boundaries of the regions where the conductivity distribution is reconstructed, are shown in Figure 4.2. It is assumed that the conductivity distribution is z invariant in each region. The conductivity distribution acquired for this case at the first iteration is shown in Figure 4.3.

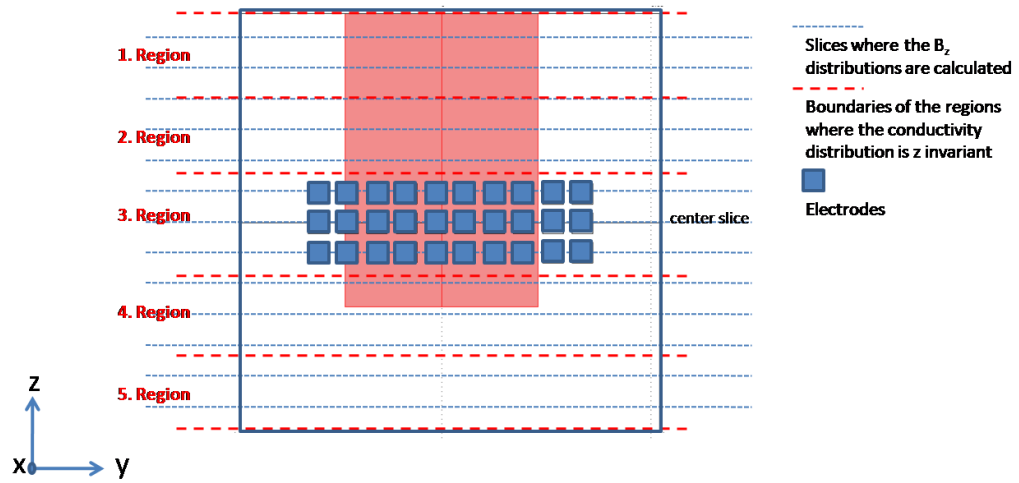

Figure 4.2 z-y cross section of the simulation phantom, the slices where the B_z's are calculated and the boundaries of the regions where the conductivity distribution is z invariant.

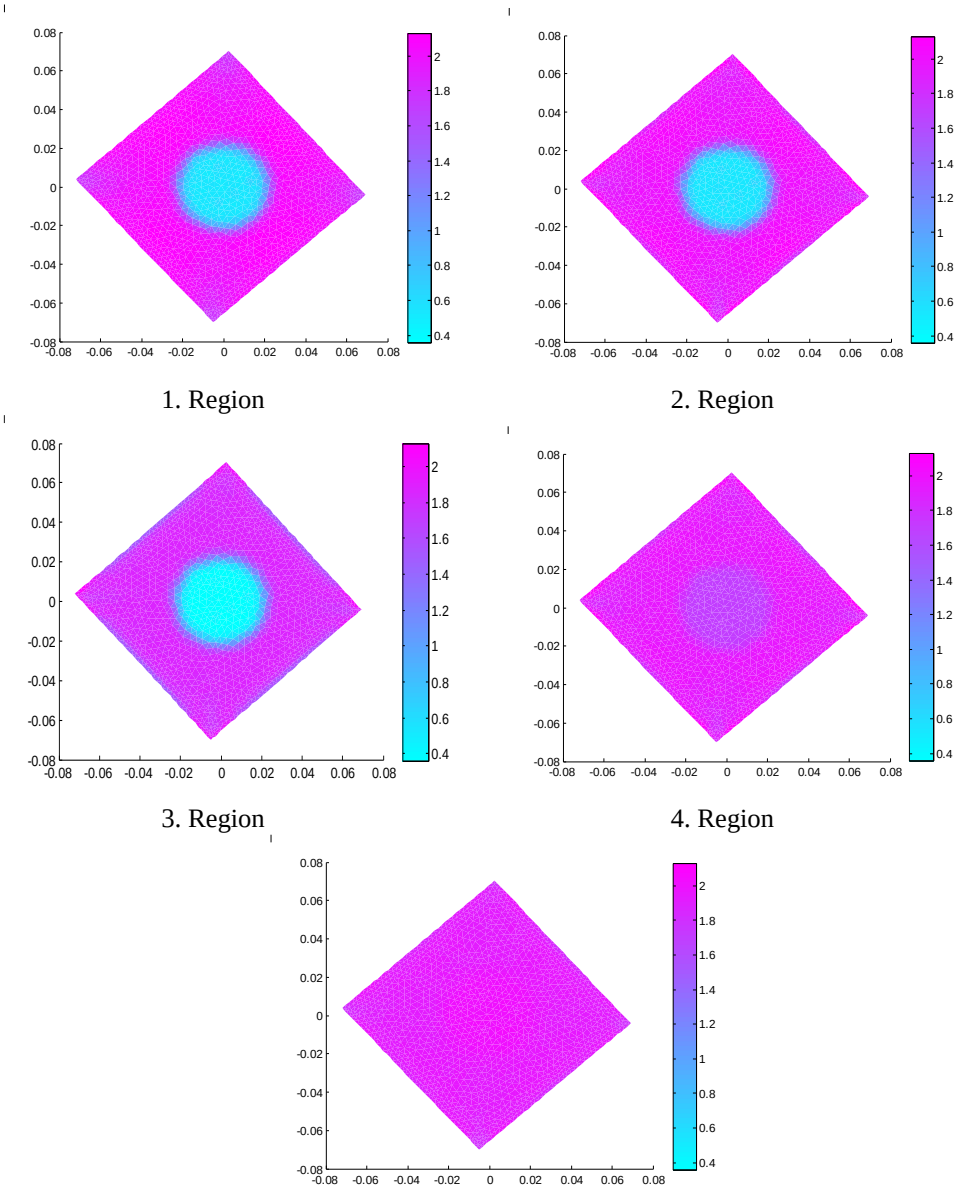

Figure 4.3 Reconstructed conductivity distribution for the first case

In the second case, magnetic flux density is again calculated at 13 different slices which are shown in Figure 4.2. However, this time it is assumed that the conductivity distribution is z-invariant for the whole object. In this case, the reconstructed conductivity distribution at the first iteration is given in Figure 4.4.

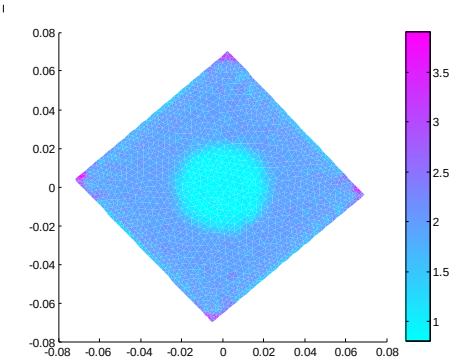

Figure 4.4 Reconstructed conductivity distribution for the second case

In the third case, magnetic flux density is calculated only at the center slice of the phantom which is shown in Figure 4.2 and the conductivity distribution is assumed to be z invariant. In this case, the reconstructed conductivity distribution is shown in Figure 4.5. In the first case the conductivity distribution found at the center slice of the phantom (3. Region) from the 13 slice magnetic flux density is very similar to the conductivity distribution acquired from the center slice magnetic flux density. These simulation results show that the if the conductivity is not changing in z direction rapidly, the conductivity distribution at a certain slice can be calculated from the magnetic flux density distribution around that slice.

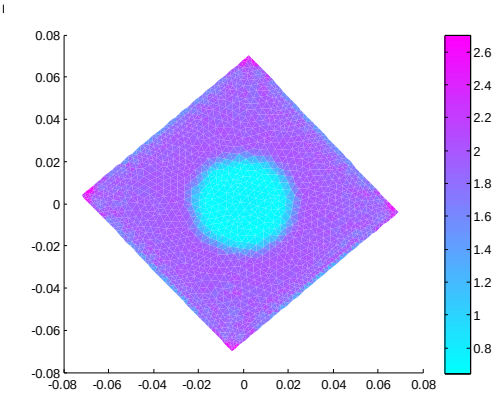

Figure 4.5 Reconstructed conductivity distribution for the third case

4.2 Simulations for Multichannel Current Source with Cubic Phantom

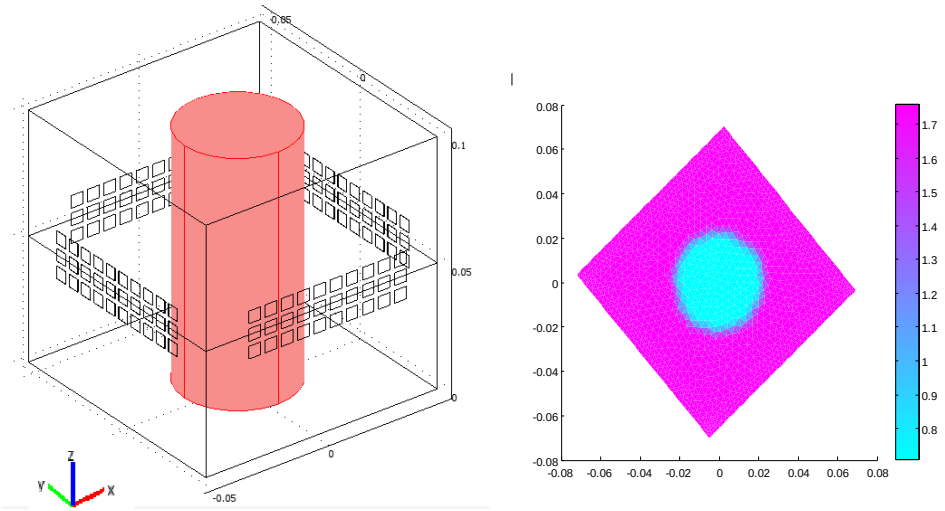

a) b)

Figure 4.6 a) Simulation phantom b) Real conductivity distribution at the center slice of simulation phantom

In order to show the performance of the multichannel current source, a cubic phantom with dimensions 10 cm is used. This phantom have multiple electrodes which are shown in Figure 4.6 on its each surface. A cylindrical object with conductivity 0.71 S/m, and background with conductivity 1.76 S/m is chosen as conductivity distribution of the simulation phantom. The real conductivity distribution at the center slice of the phantom and the position of object inside the phantom is shown in Figure 4.6. For this conductivity distribution due to the applied current from the electrodes, the z component of the magnetic flux density for two different current injection directions is shown in Figure 4.7-a&b. As the second step, z component of the magnetic flux density is recalculated for the uniform conductivity distribution (1.76 S/m). In this case, the calculated $\mathbf{B}_z$'s at the center slice for two current injection directions are shown in Figure 4.8-a&b. The calculated difference magnetic flux density $\Delta\mathbf{B}_z$'s are shown in Figure 4.9-a&b for the two current injection directions.

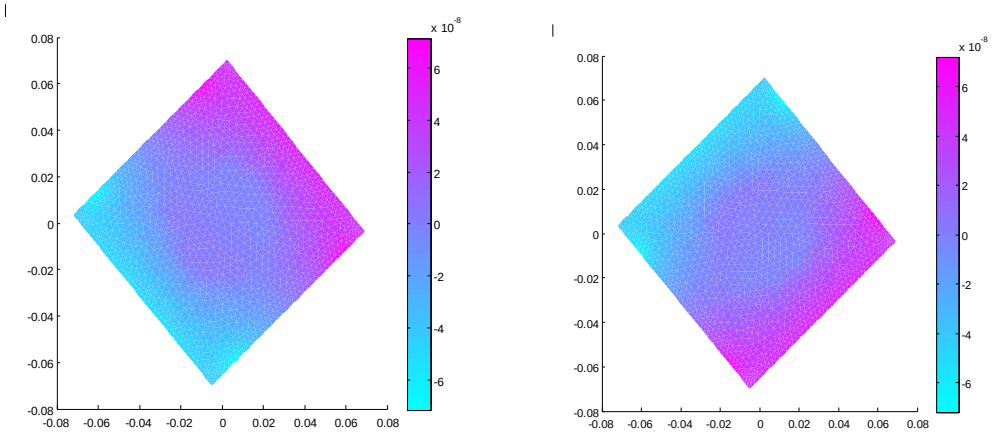

a) b)

Figure 4.7 a) Magnetic flux density for the first current injection direction and the real conductivity distribution b) Magnetic flux density for the second current injection direction and the real conductivity distribution

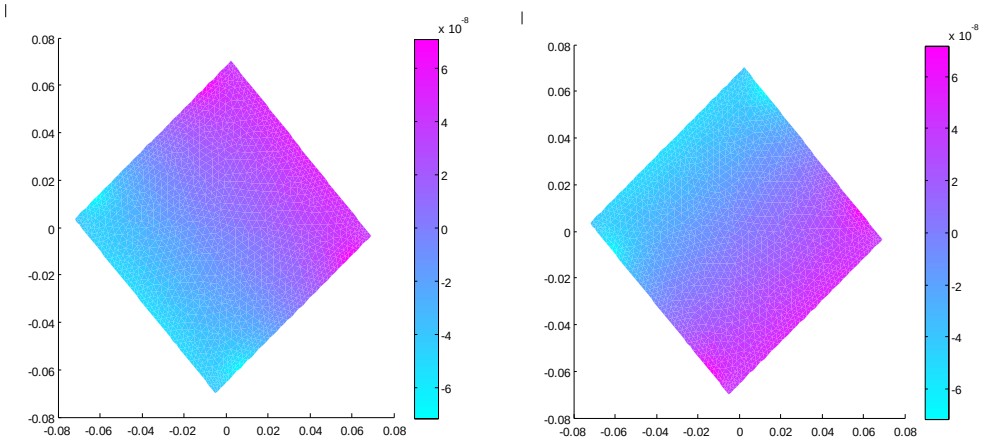

a) b)

Figure 4.8 a) Magnetic flux density for the first current injection direction and the uniform conductivity distribution b) Magnetic flux density for the second current injection direction and the uniform conductivity distribution

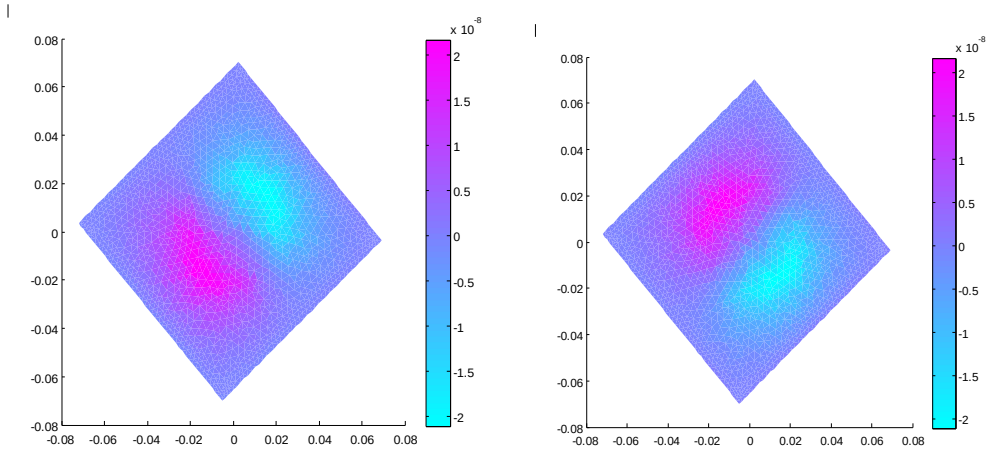

a) b)

Figure 4.9 a) Difference magnetic flux density for the first current injection direction b) Difference magnetic flux density for the second current injection direction

From the $\mathbf{B_z}$ differences in Figure 4.9-a&b the conductivity distribution at the center slice of the object should be calculated by using the $\Delta\mathbf{B_z} = \mathbf{D}\Delta\boldsymbol{\sigma}$. Here $\mathbf{D}$ matrix is a function of $\boldsymbol{\sigma}$ and if real conductivity distribution is used to find $\mathbf{D}$, calculated $\boldsymbol{\sigma}$ from $\mathbf{B_z} = \mathbf{D}(\boldsymbol{\sigma})\boldsymbol{\sigma}$ is exact. Since in the Modified Sensitivity Matrix Method $\boldsymbol{\sigma}$ is not known, it is not possible to calculate $\mathbf{D}(\boldsymbol{\sigma})$, so it is assumed to be nearly equal to $\mathbf{D}(\boldsymbol{\sigma_0}) = \mathbf{D_0}$. Here $\boldsymbol{\sigma}_0$ represents the initial uniform conductivity distribution assigned to object. So, we can calculate an estimate of $\Delta\boldsymbol{\sigma} = \boldsymbol{\sigma} - \boldsymbol{\sigma_0}$ by solving the equation below:

$$\mathbf{B_{z\_measured}} - \mathbf{B_{z\_uniform}} = \Delta\mathbf{B_z} = \mathbf{D}(\boldsymbol{\sigma})\boldsymbol{\sigma} - \mathbf{D}(\boldsymbol{\sigma_0})\boldsymbol{\sigma_0}$$

$$\Delta\mathbf{B_z} \approx \mathbf{D}(\boldsymbol{\sigma_0})\boldsymbol{\sigma} - \mathbf{D}(\boldsymbol{\sigma_0})\boldsymbol{\sigma_0}$$

$$\Delta\mathbf{B_z} \approx \mathbf{D}(\boldsymbol{\sigma_0})\Delta\boldsymbol{\sigma}$$

In order to solve $\Delta\mathbf{B_z} \approx \mathbf{D}(\boldsymbol{\sigma_0})\Delta\boldsymbol{\sigma}$ singular value decomposition is used to calculate $\mathbf{D}(\boldsymbol{\sigma_0})^{-1}$. However, since an assumption is made by taking $\mathbf{D}(\boldsymbol{\sigma_0}) \approx \mathbf{D}(\boldsymbol{\sigma})$, it is necessary to truncate the small eigen values of $\mathbf{D}(\boldsymbol{\sigma_0})$, which causes the errors in the calculation of $\boldsymbol{\sigma}$. Conductivity distribution acquired from $\Delta\mathbf{B_z}$'s in Figure 4.9-a&b by SVD with truncating the singular values of $\mathbf{D}$

matrix which are smaller than 1 percent of the maximum eigen value (tolerance=0.01) of **D** matrix is given in Figure 4.10.

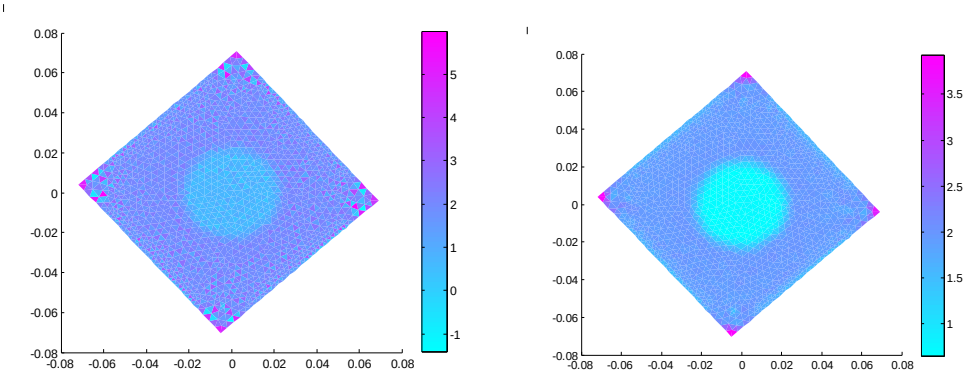

Figure 4.10 a) Conductivity distribution acquired from the ΔB_z's by SVD with tolerance 0.01 b) Filtered conductivity distribution acquired from the ΔB_z's by SVD with tolerance 0.01

Although this leads to eliminate some of the errors due to our assumption, it also causes a loss of information. This is because of the fact that small eigen values still contain detail information related to the solution. This can be shown by solving $\mathbf{B_z = D(\sigma)\sigma}$. Since in simulation we know $\boldsymbol{\sigma}$ distribution we can calculate $\mathbf{D(\sigma)}$ exactly, and solving $\mathbf{B_z = D(\sigma)\sigma}$ by SVD without any truncation gives exact $\boldsymbol{\sigma}$ (Figure 4.11-a). However, when we truncate the eigen values of $\mathbf{D(\sigma)}$ which are smaller than 1 percent or 0.1 percent of the maximum eigen value of $\mathbf{D(\sigma)}$, calculated $\boldsymbol{\sigma}$ is not exact (Figure 4.11-b&c). So, although we need to make use of truncation in SVD to get rid of the effects of noise in the data and inaccuracies in **D** matrix, this truncation results in losing some of the information to reconstruct $\boldsymbol{\sigma}$ distribution.

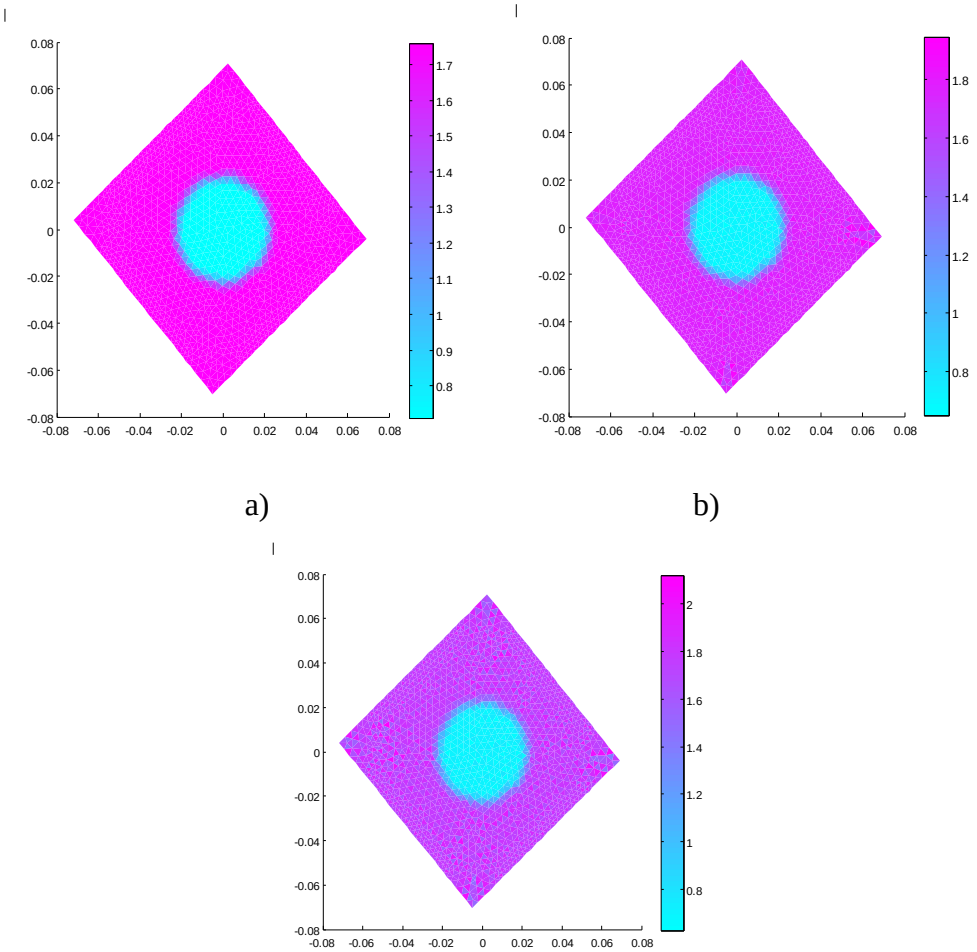

Figure 4.11 a) Conductivity distribution acquired from the ΔB_z's and the exact D matrix by SVD without any truncation. b) Conductivity distribution acquired from the ΔB_z's and the exact D matrix by SVD with tolerance=0.01 c) Conductivity distribution acquired from the ΔB_z's and the exact D matrix by SVD with tolerance=0.001

In Figure 4.10-a&b it can be seen that the calculated conductivity distribution in the corners of the phantom is faulty. This fault arises from the fact that the mesh used to solve the conductivity is loose in the corner of the phantom and the current density in these corner regions are also very low. The 2D mesh in Figure 4.13 is used to calculate the conductivity distribution instead of the mesh in Figure 4.12. In this case, the calculated conductivity distribution is given in Figure 4.14. Althouhg the conductivity distribution is better than the case which

a looser mesh is used, due to low current density the conductivity is still faulty in the corners of the phantom. This can be shown by adding new electrodes to ensure that the current density is high at this regions. Additionol electrodes are shown for one surface of the phantom in theFigure 4.15. In this case the calculated conductivity distribution is given in Figure 4.16.

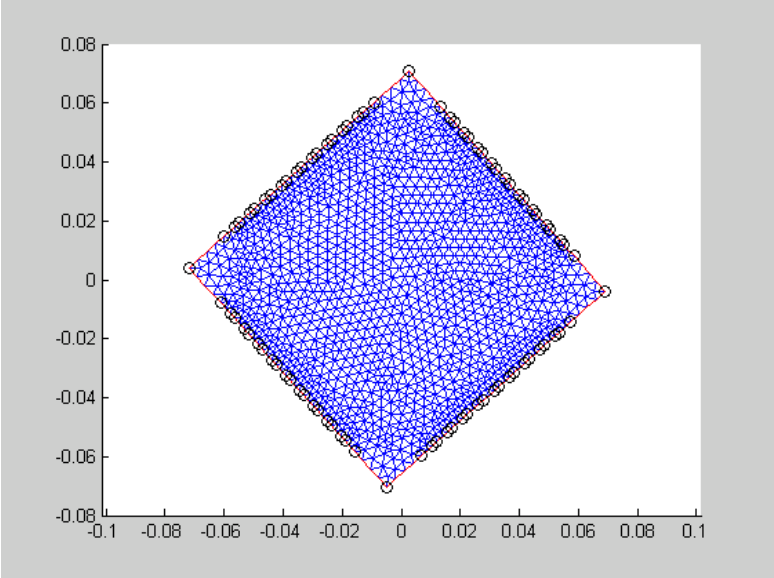

Figure 4.12 2D mesh which is used to construct 3D mesh by extrusion

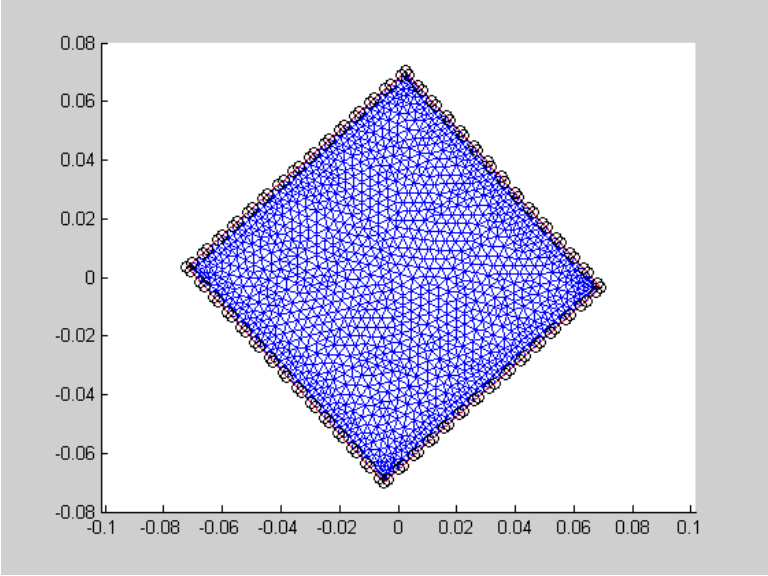

Figure 4.13 Refined 2D mesh which is used to construct 3D mesh by extrusion

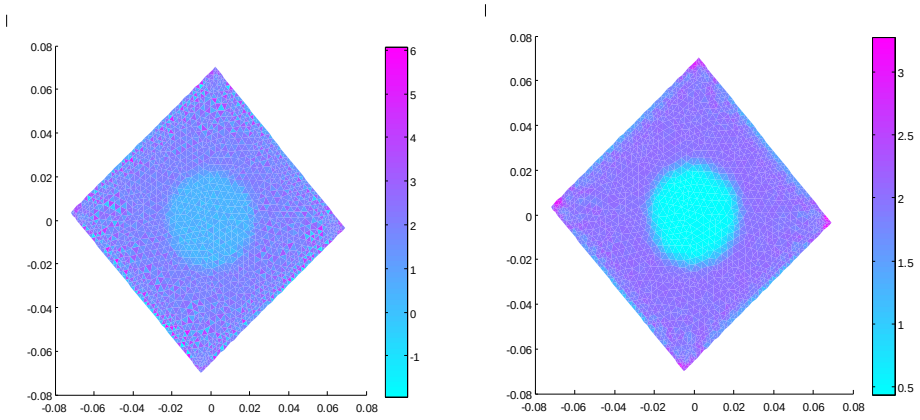

a) b)

Figure 4.14 a) Conductivity distribution acquired using the refined mesh from the ΔB_z's by SVD with tolerance 0.01 b) Filtered conductivity distribution acquired using the refined mesh from the ΔB_z's by SVD with tolerance 0.01

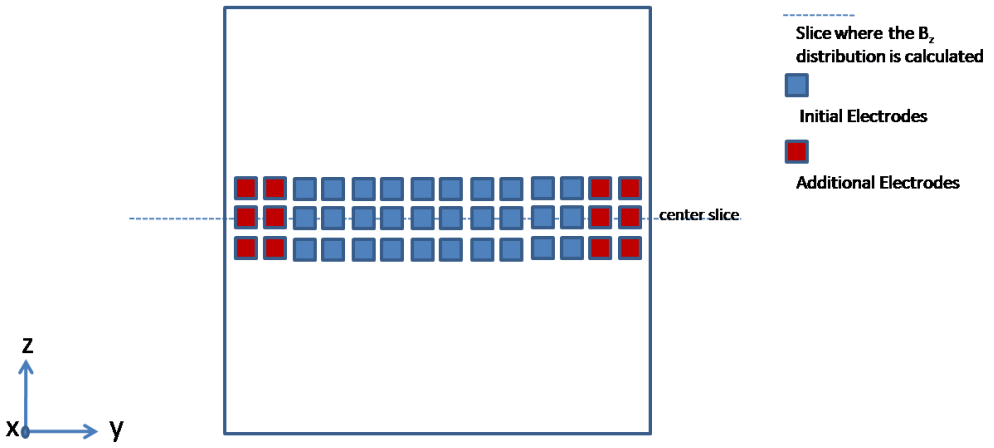

Figure 4.15 z-y cross section of the phantom and the positions of the additional electrodes

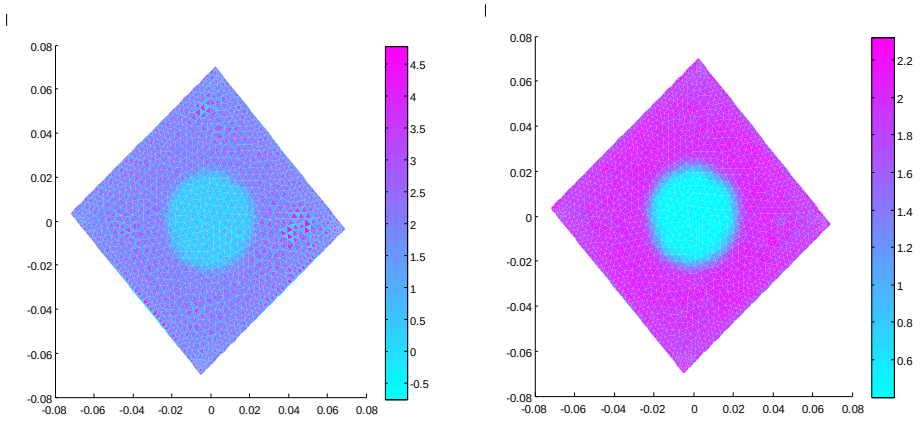

a) b)

Figure 4.16 a) Conductivity distribution acquired using the refined mesh and the extra electrodes, from the ΔB_z's by SVD with tolerance 0.01 b) Filtered conductivity distribution acquired using the refined mesh and the extra electrodes, from the ΔB_z's by SVD with tolerance 0.01

4.3 Experiment 1: MREIT experiment for an insulating object using multichannel current source

The advantages of the multichannel current source are explained in Chapter 3.3. Considering these advantages, an MREIT experiment is conducted by using a multichannel current source. First of all, a phantom with multiple electrode pairs is produced. The phantom is given at the top left of the Figure 4.17. In this figure, the square electrodes placed over the interior surfaces of the phantom can be seen. Also, outside view of the phantom can be seen at bottom left of the Figure 4.17. At the one side of the phantom there are thirty lines to carry current to the electrodes. As shown at the bottom left of the Figure 4.17, this lines are placed to be in z direction. Since the z direction is the direction of the main magnetic field of the MRI system, the current carrying lines in z direction do not produce any magnetic flux density in z direction. After producing the phantom, a balloon object filled with 1gr/L $CuSO_4$ 12gr/L NaCl solution prepared with distilled water is placed into the phantom (top left of the Figure 4.17). As a background the rest of the phantom is filled with agar solution consists of

12gr/L Agar, 12gr/L NaCl, 1gr/L $CuSO_4$ (top right of the Figure 4.17). After preparing the phantom, it is placed into the MRI system as shown at the bottom left of the Figure 4.17. MRI parameters are chosen as TR: 900 ms, TE: 60 ms, T_c= 42 ms, FOV: 150 mm, Resolution: 256*256, Slice Thickness: 5 mm. The MR magnitude image of this phantom at the center slice of the z direction is given at the bottom right of the Figure 4.17.

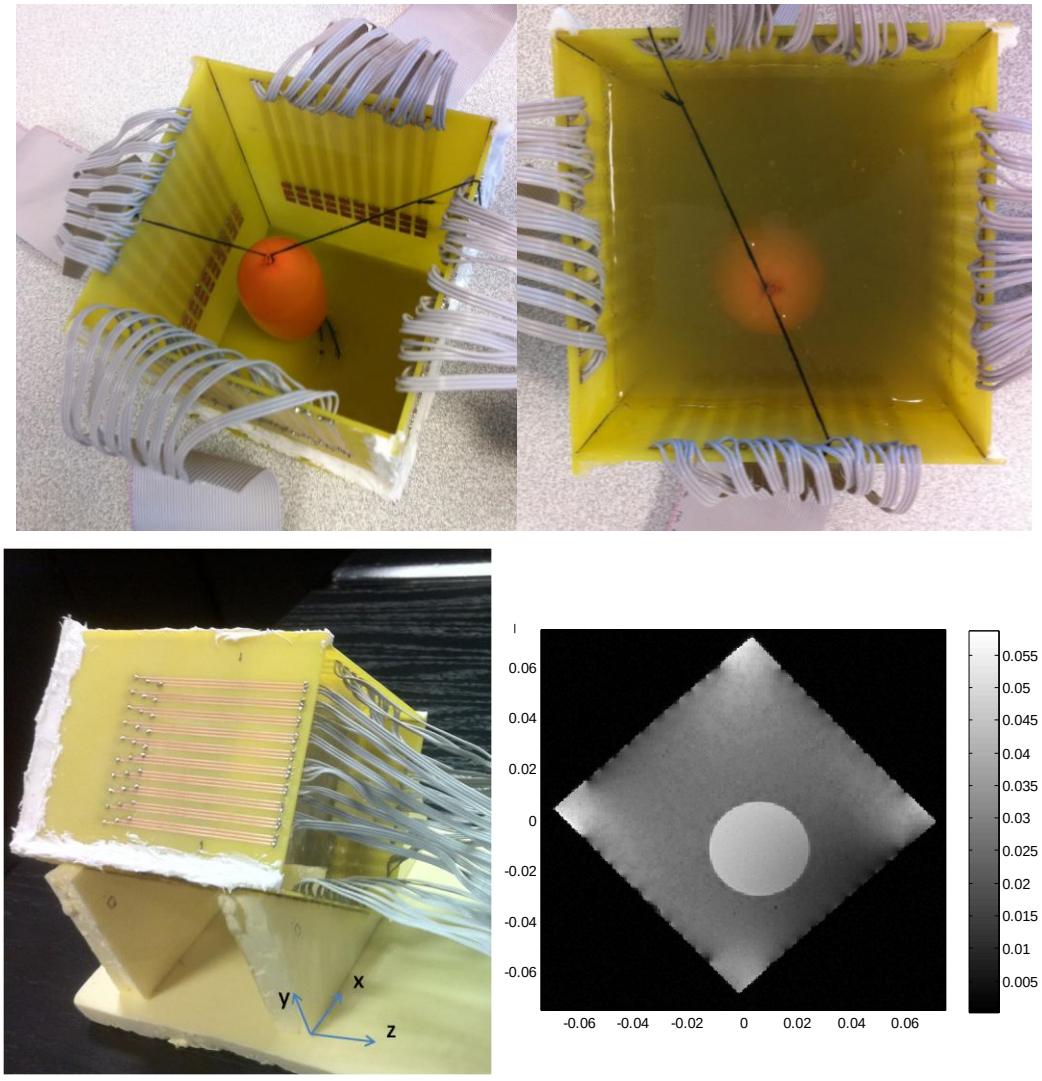

Figure 4.17 Cubic phantom with multiple electrodes and the object position inside the phantom (Top Left) outside view of the phantom and the placement direction of the phantom into the MRI scanner (Bottom Left) placement of the object into the phantom with background solution (Top Right) MR magnitude image of the center slice of the phantom (Bottom Right)

After placing the phantom into the MRI system, positive and negative currents are injected to the phantom for two different current injection directions during the MR images are taken. (The current injection directions are given in Figure 4.18). Difference magnetic flux densities (ΔB_z's) for two different current injection directions are shown in the Figure 4.19. The conductivity distribution acquired from these ΔB_z's at 5th iteration is given in the Figure 4.20.

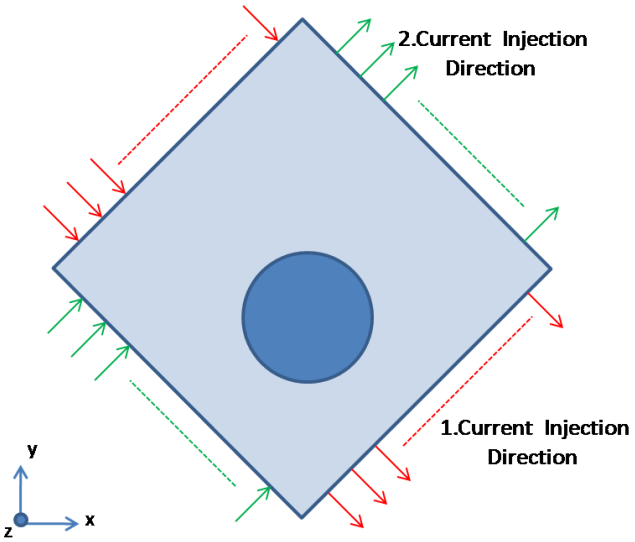

Figure 4.18 Current injection directions

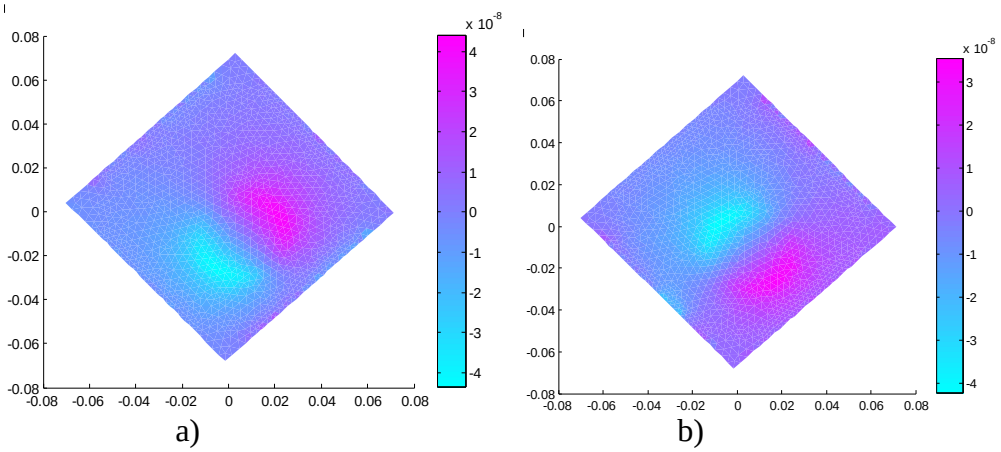

Figure 4.19 a) The difference magnetic flux density acquired for the first current injection direction b) The difference magnetic flux density acquired for the first current injection direction

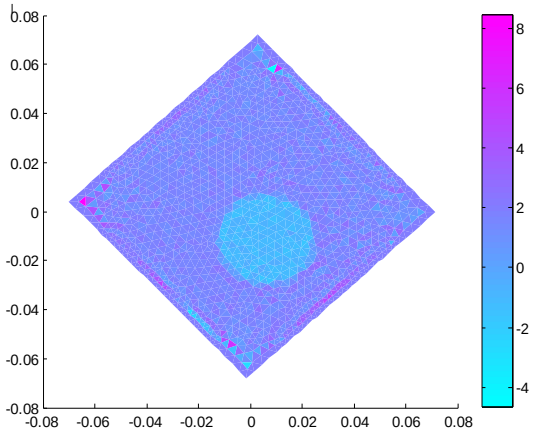

Figure 4.20 Acquired conductivity distribution for the multichannel current source experiment with a balloon object

4.4 Experiment 2: MREIT experiment for an agar object using multichannel current source

In order to conduct an experiment, a phantom shown in Figure 4.21-a is used. This phantom has multiple (30) electrodes on its' each surface. As an object a conic agar object (12gr/L agar, 3gr/L NaCl, 0.8gr/L $CuSO_4$) whose diameter varies from 3.5cm to 6cm with height 7cm is used. The conductivity of the object is measured as 0.71 S/m. After placing the object into the phantom, the rest of the space is filled with agar (12gr/L agar, 3gr/L NaCl, 1gr/L $CuSO_4$) whose conductivity is measured as 1.76 S/m. The conductivity of the object and background is measured by a conductivity meter (HANNA Instruments - HI8733). Measurements are made when the agar solutions are still in liquid form. The temperature of the agar solutions is measured as 35 C^0 by a thermometer. The position of the object in the phantom is shown in Figure 4.22. The experiment setup is shown in the Figure 4.21-b. As it can be seen from the photograph the phantom is placed into the head coil of the MRI system. MRI parameters are chosen as TR: 900 ms, TE: 60 ms, T_c= 42 ms, FOV: 150 mm, Resolution: 256*256, Number of Slices: 13, Slice Thickness: 7 mm, Slice Gap: 0. For each of the two current injection directions which are shown in the Figure 4.18, positive and negative currents whose magnitudes are 19 mA are injected to the object during the image acquisition. Since the MRI images are

acquired from 13 slices, $\mathbf{B}_z$ measurements are also acquired at 13 slices from the phase of these MRI images.

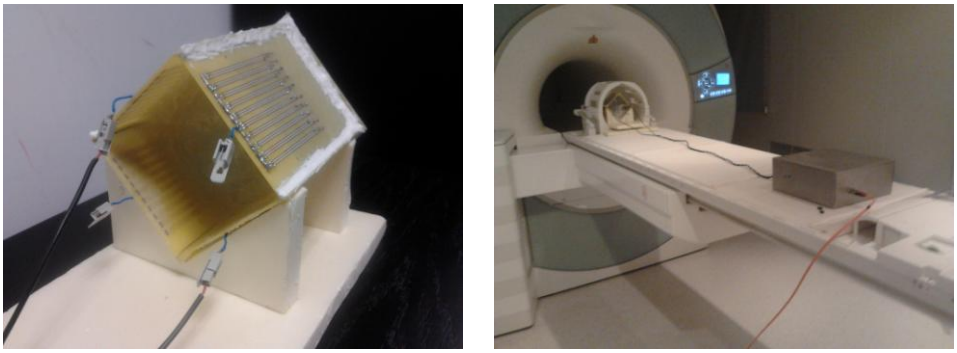

a) b)

Figure 4.21 a) Phantom for experiment b) Experiment setup for MREIT

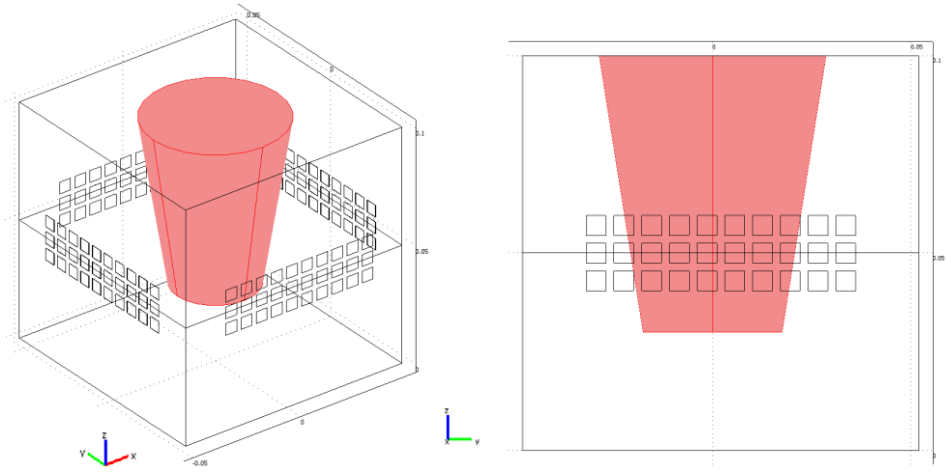

a) b)

Figure 4.22 a) Position of the object in phantom which is prepared for experiment b) z-y cross section of the phantom.

Using acquired $\mathbf{B}_z$ distribution, conductivity distribution is reconstructed for three different cases. Calculated $\Delta\mathbf{B}_z$'s at 13 slices are shown in Figure 4.27 for the two different current injection directions. First case is the reconstruction of the conductivity distribution at 5 different slices from the measured $\mathbf{B}_z$ distribution at 13 slices. The 5 regions where the conductivity distribution is calculated are shown in Figure 4.23. In each of this regions it is assumed that the conductivity distribution is z invariant. Conductivity distribution acquired for this case is shown in Figure 4.24.

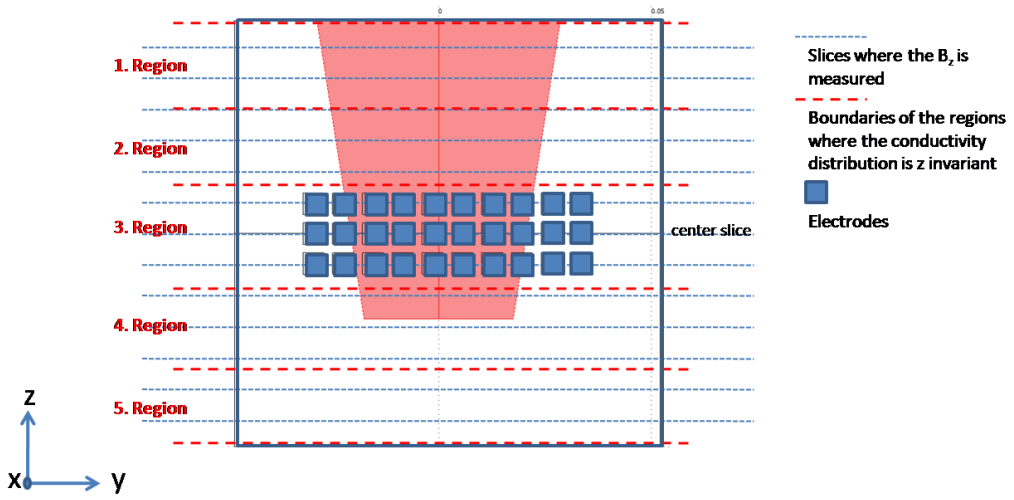

Figure 4.23 z-y cross section of the experiment phantom, the slices where the B_z's are measured and the boundaries of the regions where the conductivity distribution is z invariant.

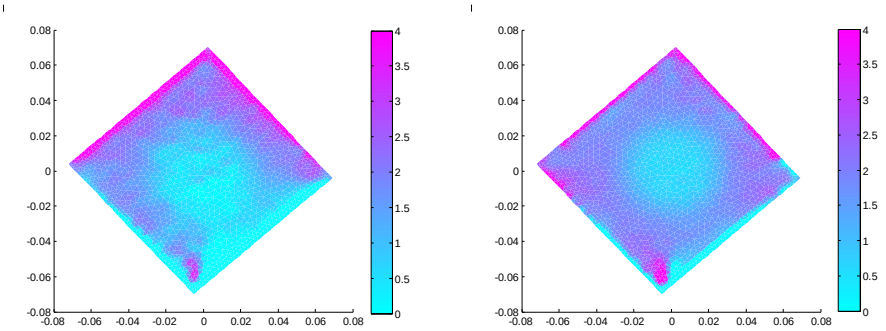

1. Region

2. Region

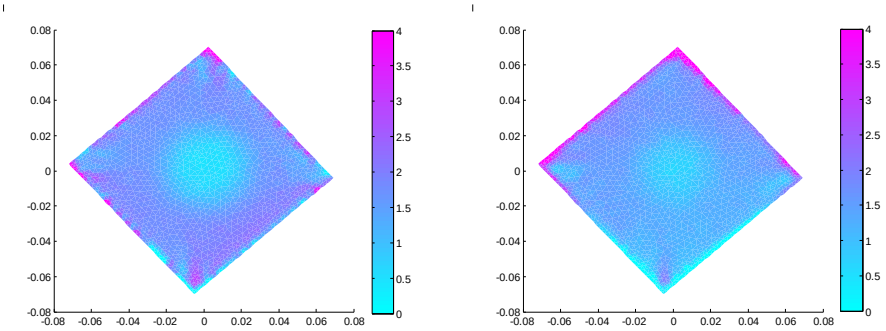

3. Region

4. Region

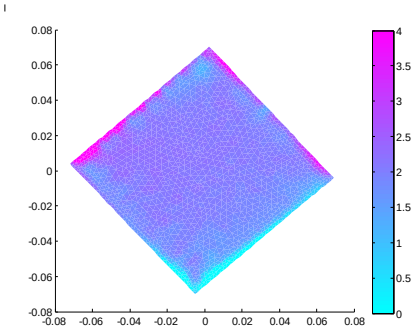

5. Region

Figure 4.24 Reconstructed conductivity distribution for the first case

In the second case, the conductivity distribution is reconstructed from the $\mathbf{B}_z$ measurements acquired at 13 different slices. However, it is assumed that the conductivity distribution in the object is z invariant. In this case the reconstructed conductivity distribution is given in Figure 4.25.

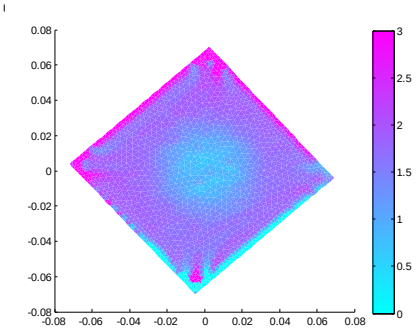

Figure 4.25 Reconstructed conductivity distribution for the second case

Finally in the third case, conductivity distribution is reconstructed from the $\mathbf{B}_z$ measured only at the center slice (7. slice) of the object. However, it is assumed that the conductivity distribution in the object is z invariant. In this case, the reconstructed conductivity distribution is given in Figure 4.26.

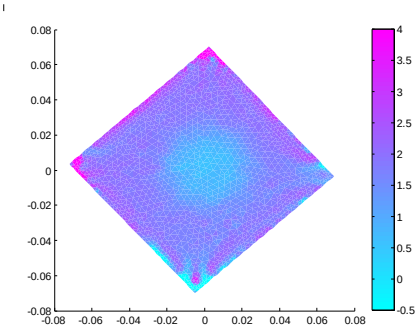

Figure 4.26 Reconstructed conductivity distribution for the third case

Reconstructed conductivities in this experiment represents the conductivity distribution of the 3D object. However, due to the noise in the $\mathbf{B}_z$ data conductivity distribution acquired at the boundary regions has errors. Since the current density in the corner regions of the object is very low, errors in conductivity distribution are especially concentrated around the corners of the object.

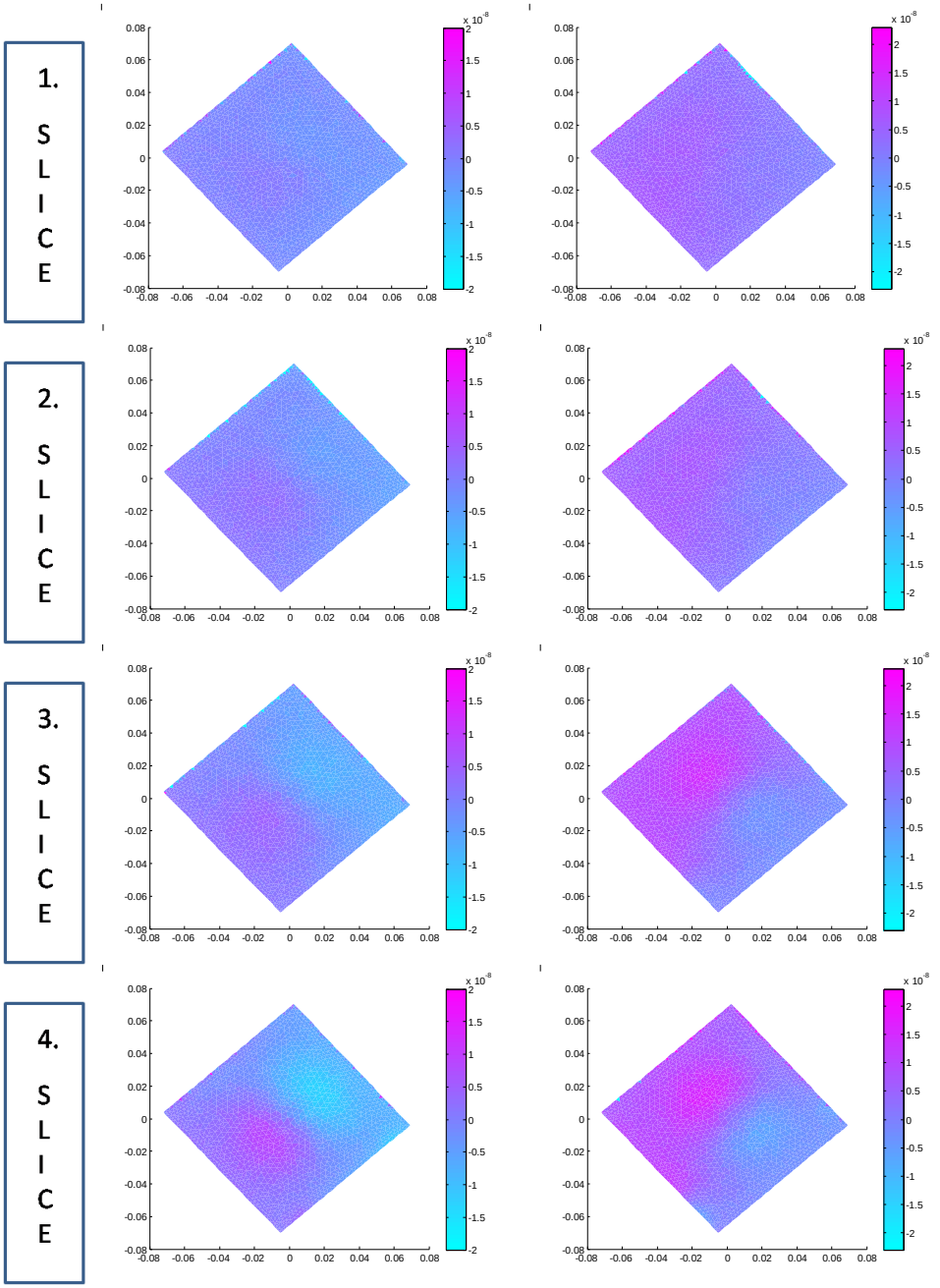

5. SLICE

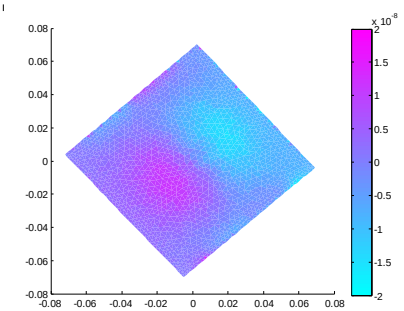
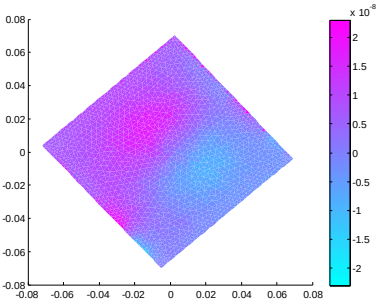

6. SLICE

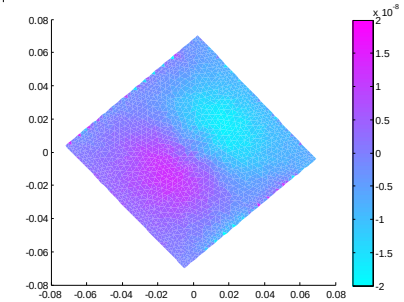
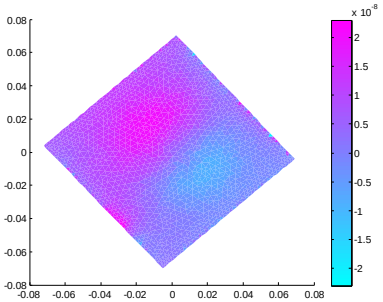

7. SLICE

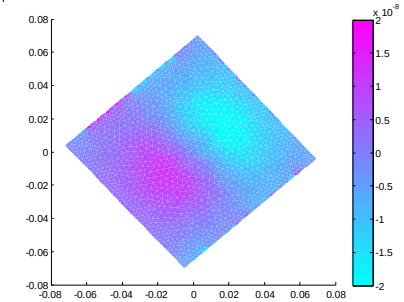
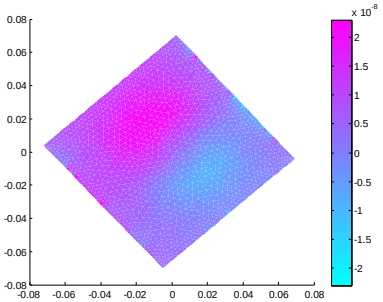

8. SLICE

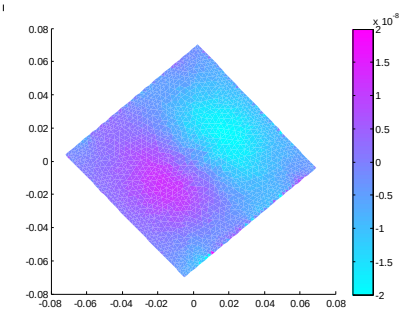
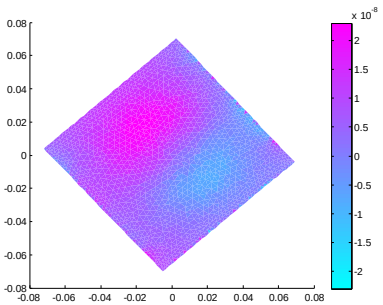

9. SLICE

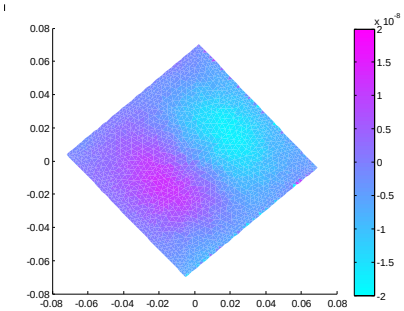
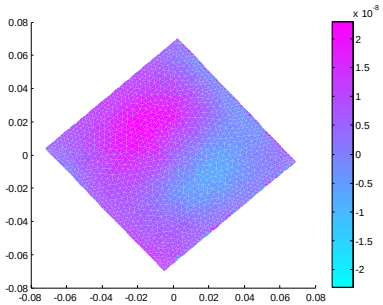

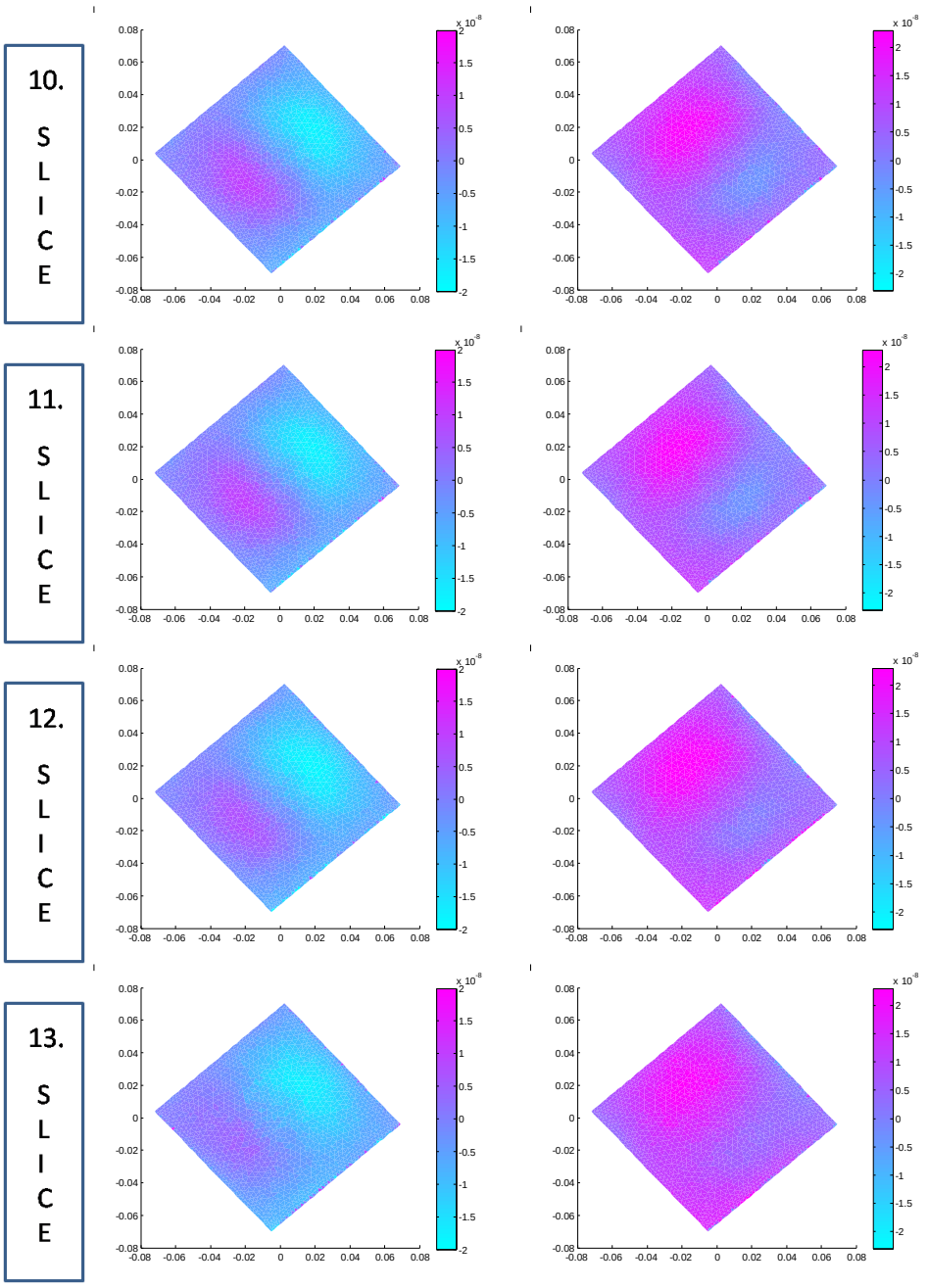

Figure 4.27 ΔB_z distributions for two current injection directions at 13 slices. (1. slice is the bottom and 13. slice is the top slice of the phantom)(ΔB_z's which are related to the 1. current injection direction are given at left side of each line. ΔB_z's acquired from the 2. current injection directions are shown at the right side of the each line.)

Chapter 5 : Conclusions and Discussions

Magnetic Resonance Electrical Impedance Tomography (MREIT) has been a research topic for about two decades. This is a technique used in order to image electrical conductivity distribution inside an object. MREIT is based on the reconstruction of the conductivity distribution from the measured magnetic flux density arising from currents injected into the object. In order to reconstruct the conductivity distribution inside the object, several conductivity reconstruction algorithms have been developed.

One of the conductivity reconstruction algorithms in MREIT is the Sensitivity Matrix Method. Three main problems related to this methods are investigated in this thesis: First of all, Sensitivity Matrix Method is not generally used in 3D problems. This is because of the fact that this method requires large memory space and long time to reconstruct the conductivity distribution. Secondly, in MREIT, use of uniform current density distribution inside the object is desirable. This is because of the fact that by using uniform current density inside the object, it is possible to reconstruct conductivity distribution with more accuracy. However, uniform current density cannot be obtained by using a single channel current source. Finally, it is necessary to calculate difference magnetic flux density ($\mathbf{\Delta B_z}$) for Sensitivity Matrix Method. If the boundaries of the model are not well matched with the boundaries of the real object during the calculation of the uniform magnetic flux density, there will be errors in the $\mathbf{\Delta B_z}$. The inaccuracies in the measurements and also the inaccuracies in calculations are the other sources of the errors in $\mathbf{\Delta B_z}$. These errors are significantly high around the electrodes where the $\mathbf{\Delta B_z}$ changes rapidly. Therefore they cause errors in the reconstruction of the conductivity distribution.

In the chapter 2.1.1 it is shown that the calculation of the sensitivity matrix for the Conventional Sensitivity Matrix Method requires the solution of the forward problem N times. Here N is the number of the finite elements in the model of the 3D object. Since the number of the finite elements in 3D objects is too many, the time required to calculate the sensitivity matrix for the Conventional Sensitivity Matrix Method will be too long. On the other hand, in the proposed Modified Sensitivity Matrix Method, only one forward problem solution is required to construct the sensitivity matrix. The conventional sensitivity matrix is given as below:

$$\mathbf{D}_C = \left(\mathbf{D}_0 + \frac{\partial(\mathbf{D}\boldsymbol{\sigma}_0)}{\partial \boldsymbol{\sigma}}\bigg|_{\boldsymbol{\sigma}_0} \right)$$

The conventional sensitivity matrix is calculated for a simulation phantom which is shown in Figure 4.1. For the calculation of the sensitivity matrix, the conductivity of the object is assumed to be z invariant so that the conductivity distribution can be assumed to be 2D. For each element in the 2D conductivity mesh, the maximum absolute value of the sensitivity of the center slice magnetic flux density to the conductivity change of the element is calculated. This calculated "sensitivity map" is given in Figure 5.1.

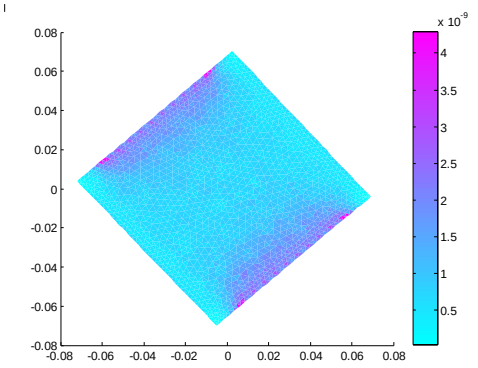

Figure 5.1 Maximum absolute sensitivity values of the center slice magnetic flux density to the change in the conductivities of each element in conventional sensitivity matrix (sensitivity map which is acquired from conventional sensitivity matrix).

On the other hand, in the modified sensitivity matrix method, $\mathbf{D}_0$ is used as the sensitivity matrix. In this case, the calculated sensitivity map from the modified sensitivity matrix $\mathbf{D}_0$ is given in Figure 5.2.

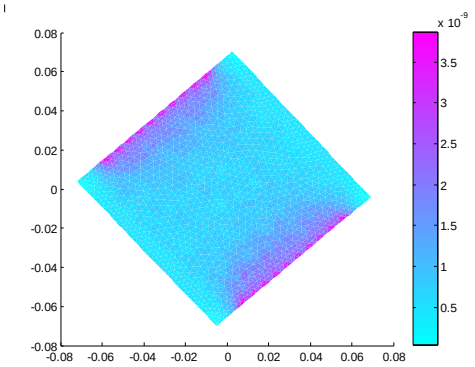

Figure 5.2 Maximum absolute sensitivity values of the center slice magnetic flux density to the change in the conductivities of each element in modified sensitivity matrix (sensitivity map which is acquired from modified sensitivity matrix).

The ratios which are obtained by dividing the conventional sensitivity map to the modified sensitivity map element by element, is given in Figure 5.3. These ratios are generally around one (0.99), throughout the object. However, it can be seen that around the boundaries, this ratio changes significantly. There are two reasons for this significant change: (i) Around the electrodes, the electric field changes too rapidly. This rapid change leads to wrong calculation of the electric field in this region. Since the sensitivity matrices are calculated from the electric field, sensitivity matrices, sensitivity maps, and the ratio of the sensitivity maps will be faulty. (ii) Since sensitivity maps may take relatively small values around the boundaries where no electrodes are placed, in these regions their ratio may not give reliable results.

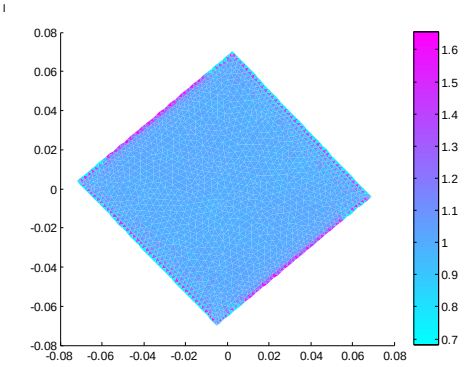

Figure 5.3 Ratio of the sensitivity maps, which is calculated element by element.

Some of the differences between the conventional and modified sensitivity matrices may be attributed to calculation errors as explained above but some of the differences are of course essential. These essential differences are the reasons for having less number of iterations in the Conventional Sensitivity Matrix Method as compared to the Modified Sensitivity Matrix Method.

Although there are errors around the boundaries as mentioned above, the ratio of the conventional sensitivity map to modified sensitivity map is around one throughout the rest of the object. Therefore, using the modified sensitivity matrix instead of conventional one should give a similar result. It was shown by simulations in Chapter 2.3.2 that the constructed conductivity distribution from both of the sensitivity matrices, converges to the nearly same solution.

In the Conventional Sensitivity Matrix Method, the calculation of the sensitivity matrix at each iteration is the most time consuming part of the algorithm. Since the calculation of the modified sensitivity matrix requires significantly less time than the conventional sensitivity matrix, the Modified Sensitivity Matrix Method is faster than the conventional one.

Although, the calculation time of the sensitivity matrix is reduced by the Modified Sensitivity Matrix Method, the dimension of the sensitivity matrix is still too large to be solved. Solving the conductivity values from such a large matrix requires both large memory space and long time. Therefore in this thesis, the dimension of the sensitivity matrix is reduced by making assumptions about the conductivity values of the finite elements. The assumptions about the conductivity values are made considering the results of the sensitivity analysis in z direction. The change in the center slice magnetic field due to the change in the conductivity of an element is defined as the sensitivity of the center slice magnetic field to the change of conductivity of that element. According to the sensitivity analysis in Chapter 2.3.1, the center slice magnetic field is only sensitive to the changes in the conductivities of the elements which are very

close to the center slice of the phantom. This means that if the finite element is not close to the center slice, assigning any conductivity value to this finite element does not change the magnetic field distribution at the center slice. Consequently, in this thesis, conductivity values of the finite elements with the same x, y coordinates are chosen such that they have the same conductivity values. After this assumption, the columns of the sensitivity matrix related to elements with the same x, y coordinates can be added to each other. Obviously, it reduces the dimension of the sensitivity matrix. This reduction leads to less memory usage, and the shorter solution time.

At the corners of the center slice of the cubic phantom, current density is very low as compared to the current density in other regions. In these regions, the values of sensitivity maps which are acquired from both conventional and modified sensitivity matrices are low. This means that the center slice magnetic field of the object is less sensitive to the change of conductivity in the elements which have low current densities as compared to the other elements. So the resolution of the reconstruction algorithm will be low in these regions. This can be verified by the results of the simulations in Chapter 4.2. In this simulation, additional electrodes placed near the corners cause higher current density in the corner regions and as a result conductivity values in the corners of the object are found more accurately. These results emphasize the importance of uniform current density inside the object for the reconstruction of conductivity distributions: Uniform current density forms a nearly uniform sensitivity map for an object. Since a uniform sensitivity map is obtained, a nearly uniform reconstruction resolution can be achieved throughout the object.

In the Sensitivity Matrix Method it is necessary to subtract magnetic flux density calculated for the uniform conductivity distribution from the measured magnetic flux density. However calculation of the magnetic field for the uniform conductivity case is problematic for objects used in real experiments: While solving the magnetic flux density for the uniform conductivity distribution, it is

necessary to define the exact boundary positions in order not to have errors in the difference magnetic flux density. However, in practice, it is not usually possible to define the boundary positions exactly. In chapter 3.1 the effects of the errors in defining the boundary are investigated. As a result of this work, it is seen that the errors in $\mathbf{\Delta B_z}$ are significantly high around the electrodes. This is because of the fact that around the electrodes the amount of the current density increases rapidly and causes rapid changes in magnetic flux density. These rapid changes in current density cause calculation and measurement errors related to the magnetic flux density. In this thesis, to overcome these problems, using a multichannel current source is proposed. The multichannel current source produces nearly uniform current density inside the object. This leads to a decrease in rapid changes of the current density around the electrodes. Since there is no rapid change in the current density, the measurement and calculation errors around the electrodes will also decrease. Therefore the errors in $\mathbf{\Delta B_z}$, which are arising from the boundary definition errors are reduced.

Appendix A

Derivation of the $\mathbf{\Delta D\sigma_0}$ *Term*

$$\mathbf{D} = [d_1 \quad d_2 \quad d_3 \quad ... \quad d_N] \quad \mathbf{\Delta D} = [\Delta d_1 \quad \Delta d_2 \quad \Delta d_3 \quad ... \quad \Delta d_N]$$

$$\mathbf{\Delta D} = \left[\sum_{i=1}^{N} \frac{\partial d_1}{\partial \sigma_i} \Delta\sigma_i \quad \sum_{i=1}^{N} \frac{\partial d_2}{\partial \sigma_i} \Delta\sigma_i \quad \sum_{i=1}^{N} \frac{\partial d_3}{\partial \sigma_i} \Delta\sigma_i \quad ... \quad \sum_{i=1}^{N} \frac{\partial d_N}{\partial \sigma_i} \Delta\sigma_i \right]$$

$$\Delta d_1 = \left.\frac{\partial d_1}{\partial \sigma_1}\right|_{\sigma_0} \Delta\sigma_1 + \left.\frac{\partial d_1}{\partial \sigma_2}\right|_{\sigma_0} \Delta\sigma_2 + \left.\frac{\partial d_1}{\partial \sigma_3}\right|_{\sigma_0} \Delta\sigma_3 + ... + \left.\frac{\partial d_1}{\partial \sigma_N}\right|_{\sigma_0} \Delta\sigma_N$$

$$\Delta d_1 = \left[\frac{\partial d_1}{\partial \sigma_1} \quad \frac{\partial d_1}{\partial \sigma_2} \quad \frac{\partial d_1}{\partial \sigma_3} \quad ... \quad \frac{\partial d_1}{\partial \sigma_N} \right] \mathbf{\Delta\sigma} \quad \text{where} \quad \mathbf{\Delta\sigma} = \begin{bmatrix} \Delta\sigma_1 \\ \Delta\sigma_2 \\ . \\ . \\ \Delta\sigma_N \end{bmatrix}$$

$$\mathbf{\Delta D} = \left[\sum_{i=1}^{N} \frac{\partial d_1}{\partial \sigma_i} \Delta\sigma_i \quad \sum_{i=1}^{N} \frac{\partial d_2}{\partial \sigma_i} \Delta\sigma_i \quad \sum_{i=1}^{N} \frac{\partial d_3}{\partial \sigma_i} \Delta\sigma_i \quad ... \quad \sum_{i=1}^{N} \frac{\partial d_N}{\partial \sigma_i} \Delta\sigma_i \right]$$

$$\mathbf{\Delta D\sigma_0} = \left[\left(\sum_{i=1}^{N} \frac{\partial d_1}{\partial \sigma_i} \Delta\sigma_i \right) \sigma_{0_1} + \left(\sum_{i=1}^{N} \frac{\partial d_2}{\partial \sigma_i} \Delta\sigma_i \right) \sigma_{0_2} + ... + \left(\sum_{i=1}^{N} \frac{\partial d_N}{\partial \sigma_i} \Delta\sigma_i \right) \sigma_{0_N} \right]$$

$$\mathbf{\Delta D\sigma_0} = \left[\sum_{i=1}^{N} \frac{\partial \left(d_1 \sigma_{0_1} \right)}{\partial \sigma_i} \Delta\sigma_i + \sum_{i=1}^{N} \frac{\partial \left(d_2 \sigma_{0_2} \right)}{\partial \sigma_i} \Delta\sigma_i + ... + \sum_{i=1}^{N} \frac{\partial \left(d_N \sigma_{0_N} \right)}{\partial \sigma_i} \Delta\sigma_i \right]$$

$$\mathbf{\Delta D\sigma_0} = \frac{\partial \left(\sum_{j=1}^{N} d_j \sigma_{0_j} \right)}{\partial \sigma_1} \Delta\sigma_1 + \frac{\partial \left(\sum_{j=1}^{N} d_j \sigma_{0_j} \right)}{\partial \sigma_2} \Delta\sigma_2 + ... \frac{\partial \left(\sum_{j=1}^{N} d_j \sigma_{0_j} \right)}{\partial \sigma_N} \Delta\sigma_N$$

$$\mathbf{\Delta D\sigma_0} = \frac{\partial \left(\mathbf{D\sigma_0} \right)}{\partial \sigma_1} \Delta\sigma_1 + \frac{\partial \left(\mathbf{D\sigma_0} \right)}{\partial \sigma_2} \Delta\sigma_2 + ... \frac{\partial \left(\mathbf{D\sigma_0} \right)}{\partial \sigma_N} \Delta\sigma_N$$

$$\mathbf{\Delta D\sigma_0} = \left. \frac{\partial \left(\mathbf{D\sigma_0} \right)}{\partial \boldsymbol{\sigma}} \mathbf{\Delta\sigma} \right|_{\sigma_0}$$

Appendix B

Boundary Detection Methods

Most of the MREIT algorithms require to solve the forward problem. Since the forward problem aims to calculate internal current density and magnetic flux density for the known boundary, we need to know the boundaries of the object. If the boundary of the object is not known, MRI magnitude images might be helpful to construct the boundary of the object. One way to get the boundary of the object from the MRI magnitude image is using the edge detection algorithms like Sobel, Canny . For example, the boundary information acquired from the MRI magnitude image given in the (Figure B. 1-a) by the Sobel edge detection algorithm is given in the (Figure B. 1-b). Sobel edge detection algorithm is applied to the MRI magnitude image by the "edge" function of the MATLAB software.

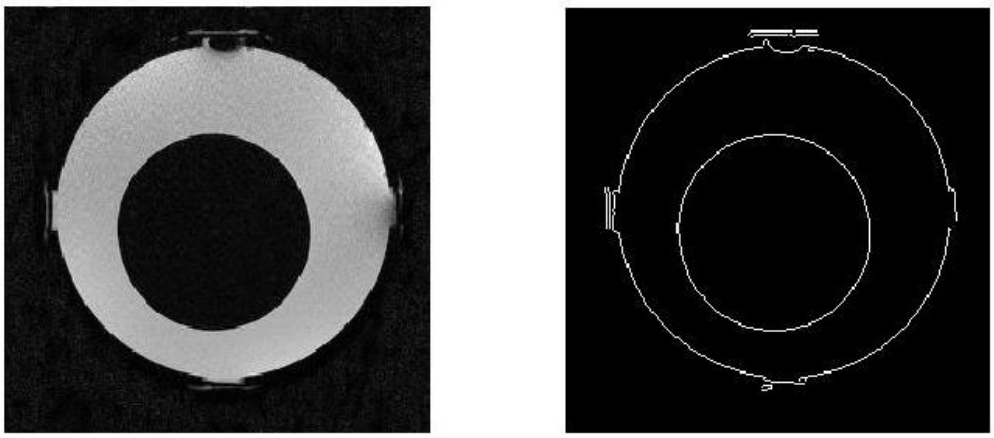

a) b)

Figure B. 1 (a) MRI magnitude image (b) boundary acquired from the Sobel edge detection algorithm

However, the edge detection algorithms cannot always find the boundary information exactly. Especially, when the signal level of the magnitude image is low, the boundary information found from the edge detection algorithms, might be wrong or missing. This is why a method which allows the user to determine the boundary of the object manually is used. In this method, first of all the boundary of the object is sampled over the MRI magnitude image (Figure B. 2).

Then from the sampling points the boundary of the object (Figure B. 3-a) can be defined by the software written in the MATLAB. This method allows the user to select the regions which are really in the region of the interest. Also, after defining the boundary nodes and edges of the object, the 2D mesh (Figure B. 3-b) for this boundary can be created using the COMSOL software. Extruding the 2D mesh gives a 3D mesh to use in the simulations.

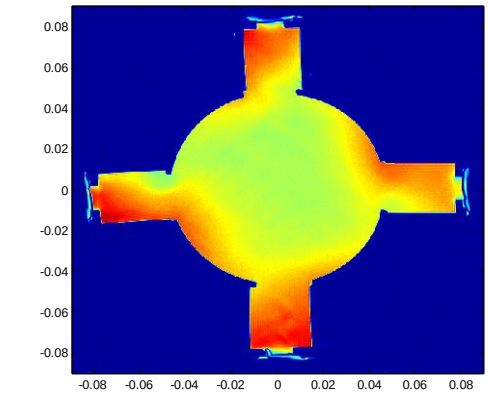

Figure B. 2 MRI magnitude image

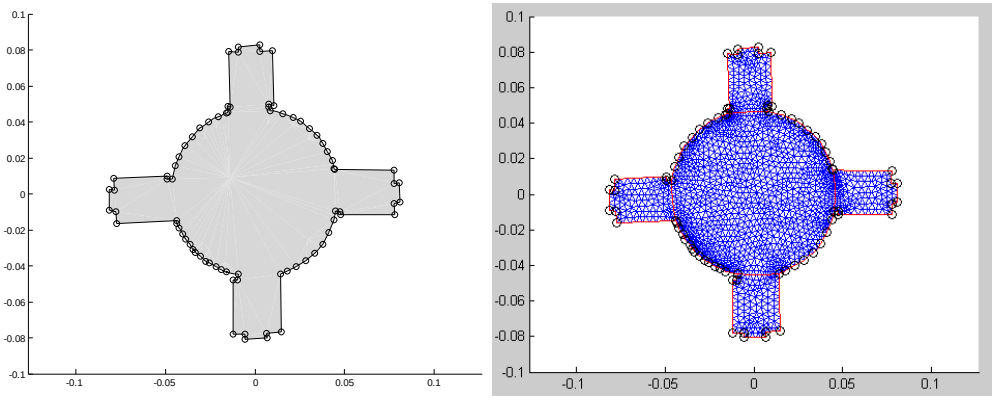

a) b)

Figure B. 3 (a) Sampling points chosen on the MRI magnitude image and the constructed boundary (b) 2d mesh produced for the constructed boundary information

BIBLIOGRAPHY

[1] A. Surowiec, S. Stuchly, J. Barr, and A. Swarup, "Dielectric properties of breast carcinoma and the surrounding tissues," *Biomedical Engineering IEEE Transection on,* vol.35, pp. 257-263,1988.

[2] S. R. Smith, K. R. Foster, and G. L. Wolf, "Dielectric Properties of VX-2 Carcinoma Versus Normal Liver Tissue," *Biomedical Engineering, IEEE Transactions on,* vol. BME-33, pp. 522 –524, 1986.

[3] D. Haemmerich, S. T. Staelin, J. Z. Tsai, S. Tungjitkusolmun, D. M. Mahvi,and J. G. Webster, "In vivo electrical conductivity of hepatic tumours," *Physiological Measurement,* vol. 24, pp. 251–263, 2003.

[4] Y Z Ider and O Birgul, "Use of magnetic field generated by the internal distribution of injected currents for electrical impedance tomography (MR-EIT)" *Elektrik Turkish J. Elec. Eng. Comput. Sci.*, vol. 6, pp. 591–604, 1998.

[5] O. Birgul, L. T. Muftuler, M. J. Hamamura, and O. Nalcioglu "3D Magnetic Resonance Electrical Impedance Tomography at 4T using Sensivity Matrix based Reconstruction" *International Society for Magnetic Resonance in Medicine*, vol.15, pp.1775, 2007.

[6] M. J. Hamamura, "Electrical Impedance Tomography Using Magnetic Resonance Imaging," Doctor of Philosophy thesis, University of California, Irvine, 2005.

[7] Y. Song, E. Lee, E. J. Woo and J. K. Seo, "Optimal geometry toward uniform current density electrodes," *Inverse Problems*, vol.27, 2011.

[8] Y.Z. Ider, "Bz-substitution MR-EIT and Fourier Transform MR-CDI: Two new algorithms," *World Congress on Medical Physics and Biomedical Engineering, Seoul, Korea*, pp. 3803-3806, 2006.